UNIVERSITÀ DEGLI STUDI DI TRIESTE

Facoltà di Scienze Matematiche, Fisiche e Naturali

Corso di Laurea in Fisica Terrestre e dell'Ambiente

Tesi di Laurea

Stratigraphic dating of Greenland glacial ice - Case study of Greenland stadial 22

Relatore: **Prof. Franco Stravisi** Laureando: **Giuliano Bertagna**

Correlatore: **Dr. Barbara Stenni**

Supervisor: **Prof. Anders Svensson**

Anno Accademico 2010-2011

UNIVERSITÀ DEGLI STUDI DI TRIESTE

Facoltà di Scienze Matematiche, Fisiche e Naturali

Corso di Laurea in Fisica Terrestre e dell'Ambiente

Tesi di Laurea

Stratigraphic dating of Greenland glacial ice - Case study of Greenland stadial 22

Relatore: **Prof. Franco Stravisi** Laureando: **Giuliano Bertagna**

Correlatore: **Dr. Barbara Stenni**

Supervisor: **Prof. Anders Svensson**

Anno Accademico 2010-2011

Abstract

In order to understand and interpret ice core records correctly, we need accurate timescales and layer-counted chronologies that we can match with independent data from different branches of palaeoclimatology. The aim of this work is to investigate the duration of Greenland Stadial 22, a cold period that occurred during last glacial, between around 84,000 and 88,000 years ago. We want to provide an estimation of this time interval, which then can be compared to other independent estimates, as that provided by the model-based timescale ss09sea and that obtained from the NALPS (Northern Alps) speleothem record.
Our counting is performed by detecting annual layers in a deep ice section of the North Greenland Ice Core Project (NGRIP), using impurities seasonal signals. The measurements were achieved with a Continuous Flow Analysis (CFA) setup at the Centre for Ice and Climate in Copenhagen. This CFA system provides high-resolution measurements that enable us to detect layers with thicknesses less than 10 mm and, thus, to count annual layers for such deep old ice, which has not been done before. Our results represent a contribution to the existing layer-counted Greenland Ice Core Chronology GICC05 that covers already the last 60.000 years, supporting the goal of extending GICC05 back to last interglacial (Eemian).

Abstract (versione italiana)

Da alcuni decenni i carotaggi realizzati nelle calotte di ghiaccio della Groenlandia e dell'Antartide rendono accessibile un prezioso archivio di informazioni legate al clima del passato, fino a centinaia di migliaia di anni fa. Esso ci consente di gettare uno sguardo sulle condizioni climatiche e sulle caratteristiche dell'atmosfera che ha contraddistinto ere passate, fornendoci degli strumenti per interpretare il clima del presente e formulare delle previsioni sulle sue possibili evoluzioni future. Per interpretare e datare le informazioni ricavate dal ghiaccio abbiamo bisogno di scale temporali il più possibile accurate. Lo scopo principale di questo lavoro è quello di analizzare una sezione di ghiaccio profondo della campagna di perforazione NGRIP (Northern Greenland Ice Core Project) realizzata in Groenlandia, al fine di fornire una stima della durata dello stadiale GS 22, un periodo freddo temporalmente localizzato durante l'ultima glaciazione, tra gli 84,000 e gli 88,000 anni fa. Infatti la durata prevista per il GS 22 dal modello ss09sea e quella recentemente stimata dall'analisi della stalagmite NALPS (Northern Alps) sono, rispettivamente, di 2900 anni e 3650 anni. All'inconsistenza tra queste due stime si aggiunge l'impossibilità di sincronizzare la carota di NGRIP e la più recente carota di NEEM (North Greenland Eemian Ice Drilling), proprio in corrispondenza dello stadiale GS 22. Per queste ragioni una stima indipendente della durata del suddetto stadiale può contribuire al miglioramento delle scale temporali in nostro possesso. Per la stima di tale intervallo di tempo si procederà ad un conteggio degli strati annui rintracciabili nel ghiaccio tramite analisi di impurità in flusso continuo (CFA, presso Centre for Ice and Climate, Copenhagen). L'utilizzo di questa metodologia ci ha permesso di risolvere strati di ghiaccio di spessore inferiore ai 10 mm, consentendo, per la prima volta, di procedere ad un loro conteggio diretto per ghiaccio così antico e profondo.

Acknowledgement

Thanks to all the people who helped me during my study and writing this work; first Anders Svensson and Paul Vallelonga for advising and for their availability; Barbara Stenni and Franco Stravisi for helping me from far away; Centre for Ice and Climate and all the people working and studying there for providing a great working environment; my family and my friends for being there.

Contents

1 Introduction **13**

1.1 Ice cores: a palaeoclimatic archive 13

1.1.1 Water isotopes and δ^{18}O 15

1.1.2 Air bubbles in ice 17

1.1.3 Impurities 18

1.1.4 Physical properties 20

1.2 The North Greenland Ice Core Project 21

1.2.1 Greenland Stadial 22 22

1.3 The NALPS record 25

2 Timescales **27**

2.1 A model-based timescale: ss09sea 28

2.2 A layer counted chronology: GICC05 30

2.2.1 Dating methods: layer counting 30

2.2.2 Building the timescale 32

2.2.3 Errors and uncertainties 36

2.2.4 Results and comparison with other timescales and reference horizons 38

3 Experimental setup **41**

3.1 Continuous Flow Analysis (CFA) 41

3.1.1 Dust 45

3.1.2 Conductivity 45

3.1.3 Sodium 46

3.1.4 Ammonium 47

4 Measurements and results 49

4.1 Sample preparation 49

4.2 Calibration of the CFA system and measurements 50

4.3 Data processing 52

4.4 Layer counting and results 54

5 Discussion and conclusions 59

5.1 Comparisons with GICC05modelext, NALPS, EDC and EDML (Antarctica) 59

5.2 Conclusions 65

Chapter 1

Introduction

What is the link between climate and ice cores? What are the mechanisms which allow us to infer information about palaeoclimate, i.e. the climate of the past years, centuries, millennia and so forth, starting from the study of the ice stored in the largest ice caps of the world, such as Antarctica and Greenland?
This first section introduces the fundamental concepts which allow us to understand the theoretical background that supports our measurements and the meaning of our results. We start with the central subject of this work: the ice.

1.1 Ice cores: a palaeoclimatic archive

Since all our measurements are made on ice drilled in Greenland, we will take Greenland as a representative example in our treatment.

The Greenland ice cap can be represented as a thin sheet (see fig. 1.1) that covers most of the island. This has a typical horizontal extension of approximately 3000 km and a maximum thickness of about 3 km. These dimensions result from a long process, in which the balance between annual precipitation and ablation plays a major role. It starts with the deposition of snow on the existing ice sheet. This snow forms a layer that can be several tens of centimeters thick and that will be covered by the snow falling down the following year. Year by year new layers form and undergo the increasing pressure of the overlying ones. This leads to a

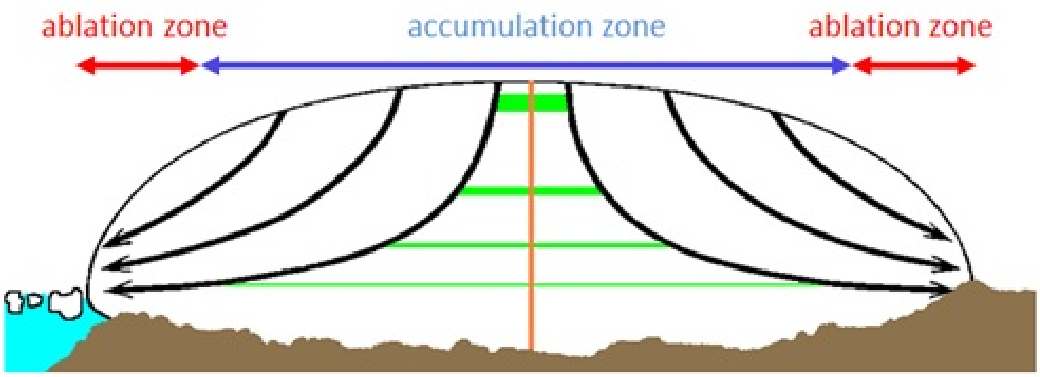

Figure 1.1: The schematic structure of the Greenland ice sheet showing the flow of ice from the top toward the bottom and the lateral margins, where it is released through ablation (melting and icebergs calving).

compressional process in the lower layers that turns snow (typical density: 50-70 kg/m^3) first into firn (up to 830 kg/m^3) and finally into ice (917 kg/m^3). This mechanism leads to two basic characteristics of the ice sheet: the first is the presence of layers that are progressively thinner as we proceed down into the ice (as in fig. 1.1). Hence, we will need a high resolution analysis to detect layers in the deepest part of the ice, which could be less than 10 mm thick. The second feature of such an ice sheet is the fact that it flows slowly but continuously, behaving like an incompressible fluid with a flow directed from the top down to the bottom and toward the lateral margins of the sheet. It means that we have to look at these regions to reach the oldest ice.

Many different factors, of course, are influencing this flow and thus the layered structure of the ice. For example one of the climatic factors is the variability of the accumulation in time and space, along different regions of Greenland. The underlying bedrock also plays a fundamental role, especially for the layers close to the bottom, which will be deformed or even folded depending on the topography of the bedrock. Another phenomenon, which actually takes place in the NorthGRIP core, is the melting of the bottom part of the ice because of a geothermal heat flux from the underlying rocks. On the one hand, this leads to the loss of the oldest layers, but on the other hand, it has the advantage of letting the remaining layers

be thicker since they are no longer pushed from below.
Now that we know how the layers are built, we can focus on what is interesting and useful about them.
Their major value is to preserve information about the past environmental and climatic conditions. What we can find in the ice can be summarized in the following four categories: the water by which the ice is made; the air bubbles (gases) trapped in it; the different kinds of impurities, as for instance insoluble dust particles; and physical properties of ice, such as its electrolytic conductivity and the crystal structure. These are all ways to infer climate information from the cores, which can be matched together to reconstruct the past atmospheric composition and characteristics. We will now briefly introduce these different palaeoclimatic sources.

1.1.1 Water isotopes and δ^{18}O

There are several different water molecules on earth, depending on which oxygen and hydrogen isotopes they are built with. Among all the possible combinations of them, only two will be taken into account for their importance here: $H_2{}^{16}O$ and $H_2{}^{18}O$. Their different weights determine the different behaviors of these molecules, leading to a weaker or stronger capacity to condense or evaporate under certain environmental conditions, among which temperature is the most important. $H_2{}^{18}O$ is heavier and for this reason it preferentially passes into the condensed phase with respect to $H_2{}^{16}O$ when forming precipitation. For the same reason, it takes a longer time for $H_2{}^{18}O$ to evaporate, compared with lighter $H_2{}^{16}O$. Therefore, a change in temperature would influence the isotopic composition of condensate and, thus, thereby of snow, leaving a fingerprint of temperature in the ice. Indeed, when water evaporates, the vapor turns out to be depleted in $H_2{}^{18}O$ (the heavier water) compared with the initial reservoir. On the other hand, when temperatures cool down, condensation takes place and the vapor loses further heavy water molecules. Hence, the more temperature decreases, the lower is the atmospheric concentration of $H_2{}^{18}O$ [Dansgaard, 1961, 1964]. δ^{18}O values in winter and summer are different because of the large temperature changes between

the two seasons, so a seasonal signal arises allowing us to count the years, as long as this signal is not obliterated by other phenomena such as air circulation across the upper layers or isotopic diffusion in the lower layers.
The isotopic composition can be described by a quantity called δ^{18}O, which has this expression:

$$\delta^{18}O = \frac{R_{sample} - R_{standard}}{R_{standard}} * 1000 \ [‰] \tag{1.1}$$

where R is the ratio between the concentration of heavy oxygen relative to light oxygen

$$R = \frac{amount\ of\ {}^{18}O}{amount\ of\ {}^{16}O} \tag{1.2}$$

and the most commonly used standard is SMOW (Standard Mean Ocean Water). Typical values of δ^{18}O in Greenland range from -45‰ to -30‰, where the most negative values are observed during colder glacial periods.

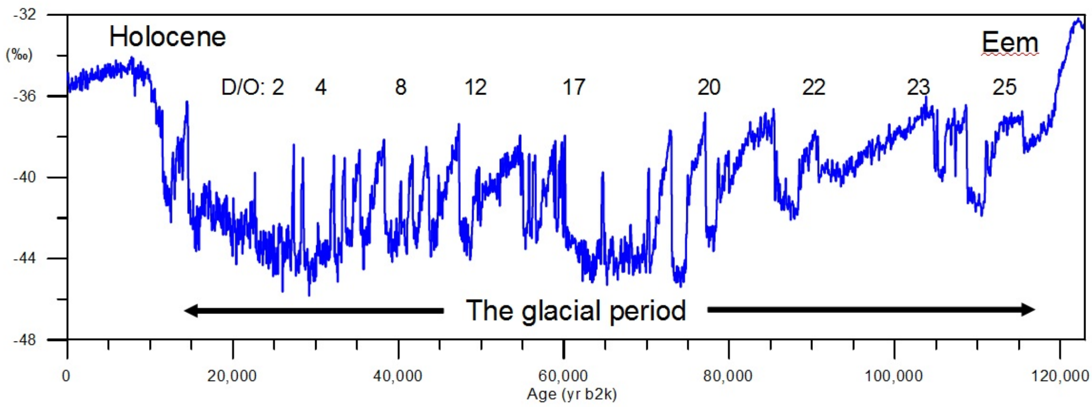

Figure 1.2: δ^{18}O profile of Greenland NGRIP ice [A. Svensson, pers. comm.].

The mechanism lying behind the isotopic composition of ice is quite complex and involves many different factors. This inverse problem is one of the targets of palaeoclimatology and δ^{18}O represents one of the most powerful proxies we know [Dansgaard, 1953, 1964]. The δ^{18}O profile obtained from the NGRIP ice core in Greenland is shown in fig. 1.2, plotted on a depth scale (and linked to time using a model). We can see that this core covers about 123 kyr, the time interval from the

late Eemian (previous interglacial period) to present, i.e. Holocene (the current interglacial). In between during the glacial period we can observe 25 Dansgaard-Oeschger events[1] of last glacial reproduced in detail. Among them we can find GS 22 (Greenland Stadial 22), which we will investigate later.
Another investigated parameter, analogous to δ^{18}O, is an expression for the Hydrogen isotopic composition, called δD.

1.1.2 Air bubbles in ice

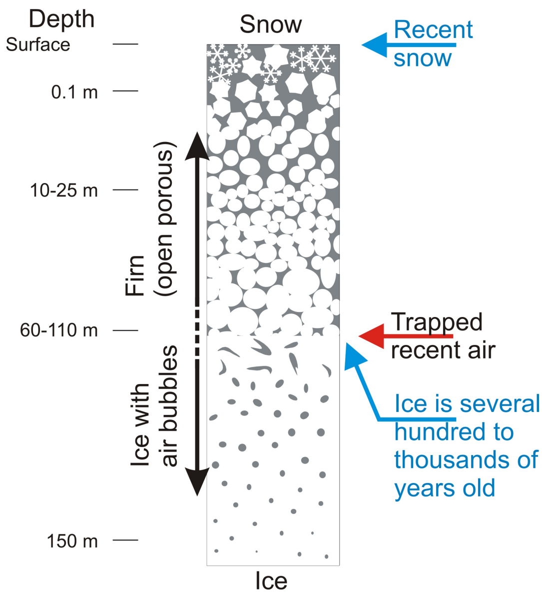

Figure 1.3: Scheme of the densification process that transforms snow into ice, first passing through an intermediate stage called firn.

As mentioned, deposited snow goes through a densification process in which its density increases until it becomes ice. When snow falls, air gets trapped by snow flakes. The more the snow densifies, the more difficult it becomes for air to move and mix with younger air from the upper freshly deposited layers and from the atmosphere. At a certain depth, which in Greenland lies around 80 m from the

[1] Dansgaard-Oeschger (D-O) cycles are very abrupt and strong climate signals with large transitions in temperature. They have been observed in many different records, such as ice cores but also speleothems (stalagmites).

surface, firn reaches a density of 830 kg/m^3, becoming ice and preventing further circulation of air, which gets enclosed in bubbles (see fig. 1.3). From now on, trapped air and ice will flow together. However, since air has been circulating and the older air mixes with younger air in the upper 70-100 meters, it turns out that the ice and the air trapped within it, they do not have the same age. The time shift between the two ages is basically preserved throughout the ice flow, but it is not constant along the whole core, as it depends mostly on the accumulation rate. Thanks to this enclosing process, ice layers carry a chemical and physical fingerprint of the atmosphere at the deposition time [Langway, 1967, Stauffer et al., 1985, Dibb and Jaffrezo, 1997]. Greenhouse gases - such as CO_2 and methane - play a very important role for climate, as they are directly involved in global warming. Methane is a well-mixed gas that can be used to synchronize signals in the two hemispheres and hence it is used as a link between ice cores from Greenland and Antarctica.

1.1.3 Impurities

Under the label "impurities" we find different kinds of microparticles, such as ions and trace elements in general, but also dust particles. The seasonal variability of these particles provides an alternative method to count layers instead of the isotope method. While water diffuses in deep ice, causing a weakening of the isotope signal, microparticles do not because of their larger size.
We will now have a look at sources and transport of the impurities we will detect later.
One of the most interesting proxies we can find in ice is dust (windblown mineral aerosols). With our analysis we will detect insoluble particles concentration, but there are also other proxies for dust, as the ion Ca^{2+}. We know that dust shows usually a maximum in early spring [Hammer, 1989], due to the stronger air circulation between winter and spring, and a minimum in autumn. Dust also shows different concentrations between warm and cold climatic periods. The latter are characterized by dry climate and strong winds, which deposit much more dust on the ice compared with the former (we can find concentrations 50 to 100

times greater in glacial stadials, i.e. cold periods) [Ruth et al., 2008]. Also the particle size distribution shows variations from warm to cold periods, due to differences in the atmospheric transport of the particles. The Sr (Strontium) and Nd (Neodymium) isotopic composition of dust recovered in Greenland ice suggests low latitude deserts of east Asia as a major dust source for this region [Biscaye et al., 1997]. Moreover we have to consider that dust is influenced also by local climatic conditions and its concentration could vary moving from one site to another within Greenland.

A first indicator for the presence of dust layers or other impurities in ice is the visual stratigraphy. In practice this is a picture of the whole ice core section, made by a line scan that uses particle scattering to detect insoluble dust or detect changes in the crystal structure, which will look differently depending on whether we are analyzing glacial or interglacial ice. Visual stratigraphy is partially visible to the naked eye, at least some of the dust layers are, and it also shows where breaks in the core are, enabling researchers to choose the best cores for their analysis.

Another species of interest is the Sodium ion Na^+. For ice sheets the main source of Na^+ is the sea salt from open ocean dispersion and from sea ice. The amount of Na^+ that we find in our records depends on the source variability and on its transport efficiency. Hence it is influenced by cyclonic activity and wind speed [Fischer et al., 2007]. As Na^+ in ice is also connected to climate conditions in the source region, it mainly represents storms and meteorological activity above the ocean. Sea salt reaches ice sheets through both wet and dry deposition, the former proportional to snow fall accumulation, the latter independent from precipitation. All these factors eventually lead to much larger loads of Na^+ during glacial periods than during interglacial ones.

Lastly we mention Ammonium, NH_4^+, which will also be detected with our CFA-setup (CFA: Continuous Flow Analysis, see section 3.1). Ammonium is mostly provided by biomass burnings (up to 40% of the total amount in Greenland during the Holocene) and in the case of Greenland it has the northern part of North America as a main source [Fuhrer et al., 1996]. Other NH_4^+ emissions arise from the soil and vegetation, building the so-called background concentration in ice

[Fuhrer et al., 1996], and from anthropogenic sources. Later we will describe how these impurities are detected by the CFA-setup.

1.1.4 Physical properties

A further approach to ice is to measure relevant physical properties such as its conductivity, which is the ability to conduct electricity and which depends on charged impurities contained in ice. A first estimate of it is made in the field, immediately after the drilling and cutting stages, measuring the so called ECM (Electrical Conductivity Measurement). ECM is a measure of the surface conductivity of the core and gives a first-approximation of the content of H^+ ions in the ice, i.e. its acidity. In fig. 1.4 it is shown how ECM is measured.

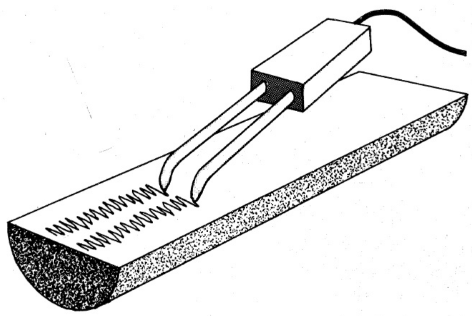

Figure 1.4: ECM (Electrical Conductivity Measurement) is measured by putting a pair of anode and cathode on the flat surface of ice and moving them slowly along the core, thus, providing a continuous ECM record [Hammer, 1980].

Other studies are made on the structure of ice crystals, whose size and orientation can provide a reconstruction of the flow history of the glacier. Also the ice temperature is measured along the borehole section, as a proxy for palaeotemperature.

1.2 The North Greenland Ice Core Project

The North Greenland Ice Core Project (NGRIP), which took place from 1996 to 2003 (when it finally reached the bedrock), followed other drilling campaigns, among which GRIP and GISP2 are the most recent ones. These two older records show some disturbances in the bottom of the cores, where the ice seems to be folded close to the bedrock, because of the bedrock morphology. This means that the data older than 105,000 yr, including the last interglacial period (the Eemian), are disturbed [Grootes et al., 1993, Fuchs and Leuenberger, 1996]. Therefore, a new drill site - NGRIP (see fig. 1.5) - was selected in order to satisfy three main requirements: it should be located on a ridge in order to reduce deformation by ice flow; it should present a flat bedrock (this point was verified by making detailed radar soundings) to minimize possible folding effects; and it should be preferably characterized by a low precipitation rate.

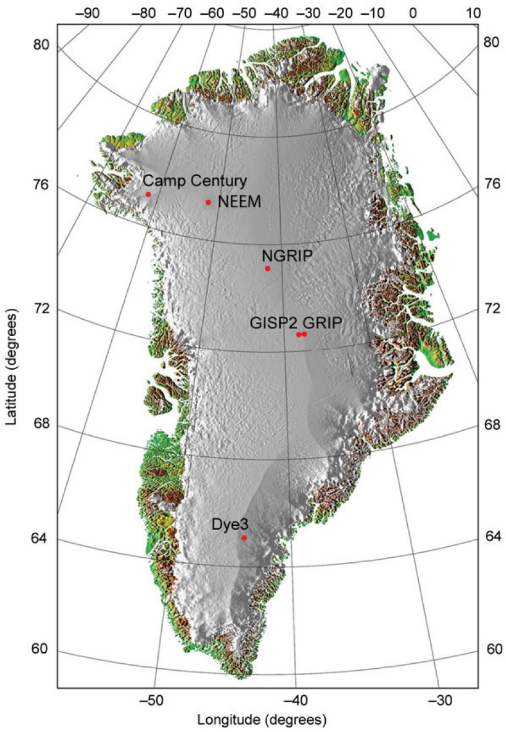

Figure 1.5: Map of Greenland, showing the locations of the deep ice core drilling sites (NGRIP-members et al. [2004] modified).

After analyzing the extracted ice, it became clear that the thicknesses of the annual layers, were larger than expected from the ice flow model, especially in the lower part of the core. The reason for that is the presence of a considerable geothermal flux arising from the bedrock that causes melting of the bottom ice, with a melt rate reaching an estimated value of 7 mm/yr [Dahl-Jensen et al., 2003, Grinsted and Dahl-Jensen, 2002]. If on the one hand this leads to the loss of the bottom older layers, on the other hand we gain an almost undisturbed chronology for the previous period, i.e. back to the late Eemian. The characteristic of this record is therefore the thickness of the layers, that, even close to bedrock, at an age of 105 kyr BP[2], is about 1.1 cm (twice the corresponding annual layer thickness in the GRIP core, for example) [NGRIP-members et al., 2004]. Figure 1.6 shows how the basal melting at the NGRIP site affects the vertical stratigraphy in terms of thickness of the lowest layers.

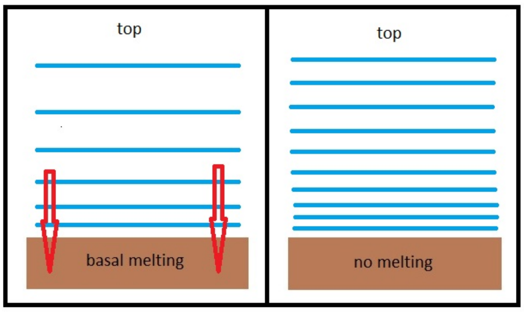

Figure 1.6: Comparison between two configurations: with and without basal melting.

1.2.1 Greenland Stadial 22

There are several reasons for the sample selection for this study that includes the end of GI 22, the entire GS 22 and the beginning of GI 21[3]. In the next

[2] Kyr BP means thousands of years before present, where year 1950 is used as the present.

[3] GI: Greenland Interstadial; GS: Greenland Stadial. The number refers to a stratigraphy of the Dansgaard-Oeschger events of the last glacial in Greenland. Cold periods, which start with abrupt climate transitions (respectively a cooling and a warming transition), are called Stadials (GS), while short warm periods preceding and following them, are called Interstadials (GI).

chapter (dedicated to the timescales), we will see that there is a layer-counted chronology (GICC05[4]) which goes back to 60 kyr b2k[5]. For older ice the only available timescale, which is called ss09sea, is based on an ice flow model. This

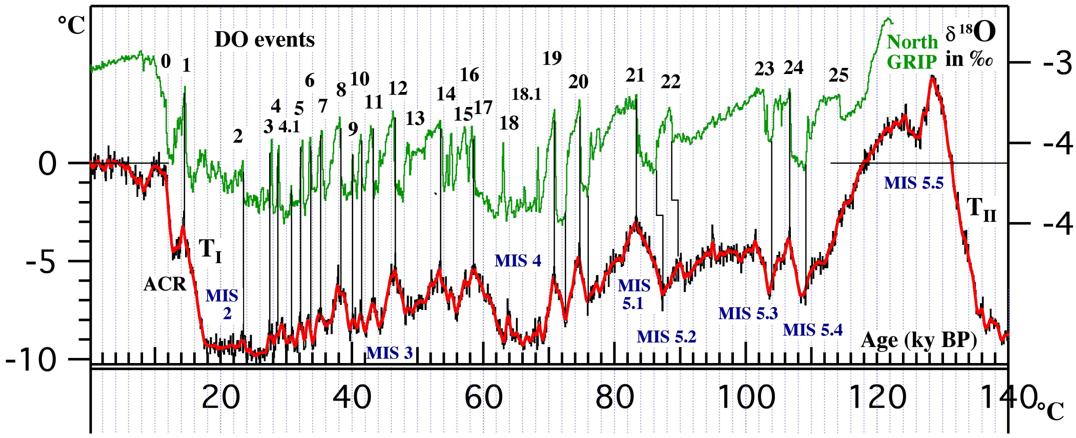

Figure 1.7: The δ^{18}O profile of NorthGRIP and the temperature change profile of EPICA Dome C (an ice core from Antarctica) are shown here. A correspondence between Dansgaard-Oeschger events in Greenland and the Antarctic Isotope Maxima (AIM) seems to exist, supporting the hypothesis of the thermal bipolar seesaw [Stocker and Johnsen, 2003]. Figure modified from [Jouzel et al., 2007]

timescale predicts for GS 22 a duration of roughly 3000 yr while comparisons to Antarctic records (figure 1.7) suggest that this period may be either shorter or longer by up to 1000 years, depending on the interpretation [Jouzel et al., 2007] or [Capron et al., 2010]. Recently another independent estimate of the duration of GS 22 was provided, which is based on the analysis of stalagmites from the Northern Alps. This is inconsistent with the model-based timescale ss09sea and suggests a duration of around 3650 years (figure 1.11, [Boch et al., 2011]), about 20% longer than the one provided by ss09sea. In addition new data from the NEEM drilling campaign[6] show a lack of tiepoints in the NGRIP-NEEM matching at depths corresponding to GS 22 and the absence of ECM tiepoints in that interval (fig.

[4] GICC05 stands for Greenland Ice Core Chronology 2005.
[5] Thousands of years before year 2000 AD.
[6] The NEEM Project, which started in 2008 and reached bedrock in 2011, had the main aim to provide a record of the entire last interglacial, i.e. the Eemian.

1.9).

The estimate provided by our CFA measurements, based on a direct counting of

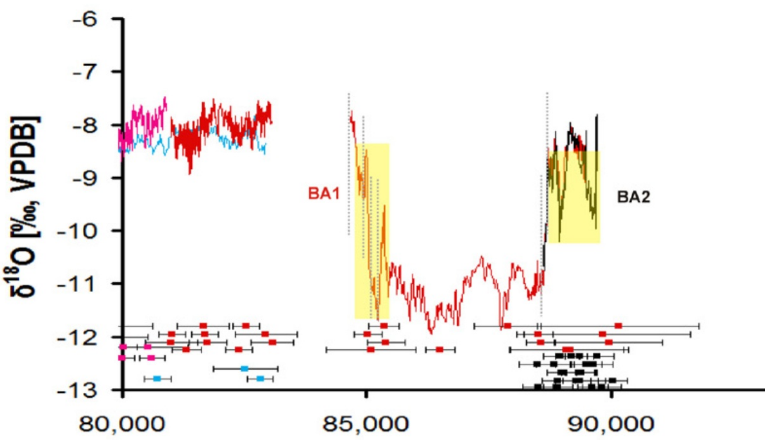

Figure 1.8: Greenland Stadial 22 as recorded by the NALPS stalagmites BA1 and BA2, modified from [Boch et al., 2011]. The horizontal error bars on the bottom represent the uncertainties related to the U-Th dating method. The yellow areas highlight sub-Dansgaard-Oeschger warming and cooling events.

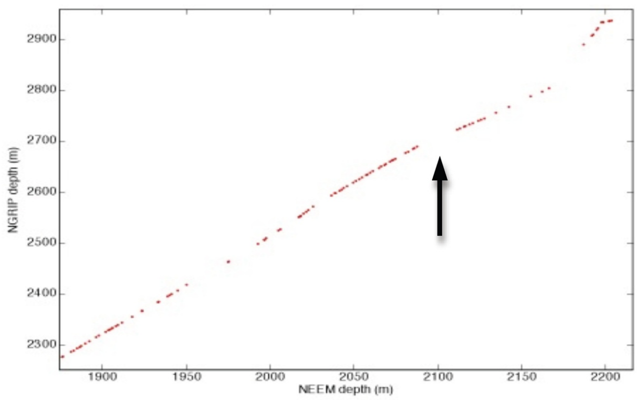

Figure 1.9: NEEM-NGRIP depth-depth matchpoint correlation over the early part of last glacial [S. Rasmussen, pers. comm.].

the annual layers in the ice, should therefore shed light on the actual duration of GS 22 and contribute to the construction and perhaps completion of the GICC05 chronology. It may also either validate the model-based timescale ss09sea, or improve it, suggesting a different tuning of its parameters.

1.3 The NALPS record

Recently, a record of several dated stalagmites from the northern rim of the Alps has been published by Boch et al. [2011]. It is composed by stalagmite sections from four different sites (see fig. 1.10) and it covers the time interval 60-120 kyr, although with some interruptions (see fig. 1.11). In the investigated time interval, also GS 22 is included, and it has been dated on two stalagmites (BA1 and BA2 in fig. 1.8), by radiometric U-Th dating.
In section 5.1 we will compare the results presented by Boch et al. [2011] to the measurements provided by the CFA system.

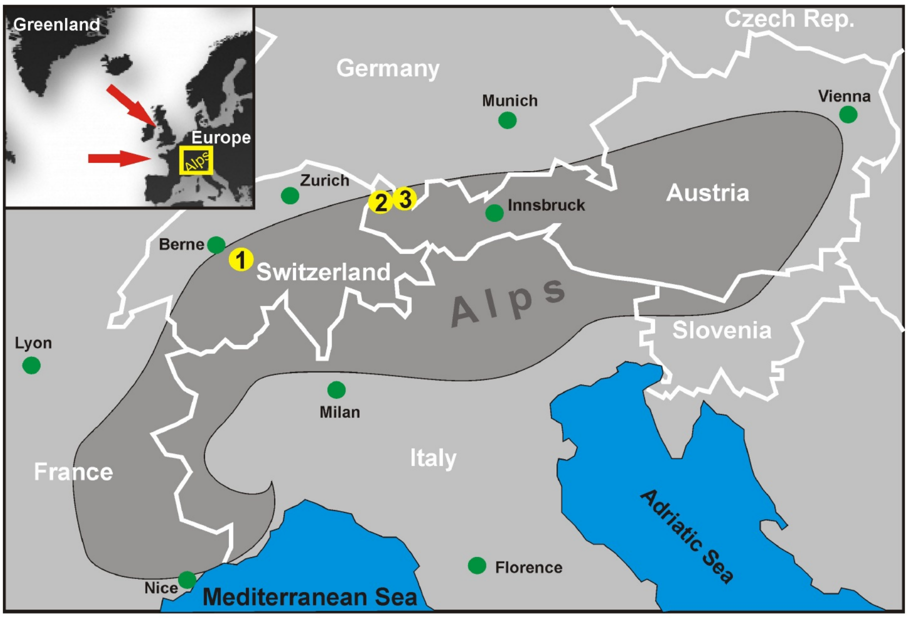

Figure 1.10: Map of the Alps showing the locations of the cave sites investigated by Boch et al. [2011]. Because of its exposure to a strong Atlantic influence, this region is suitable for a comparison with Greenland climate.

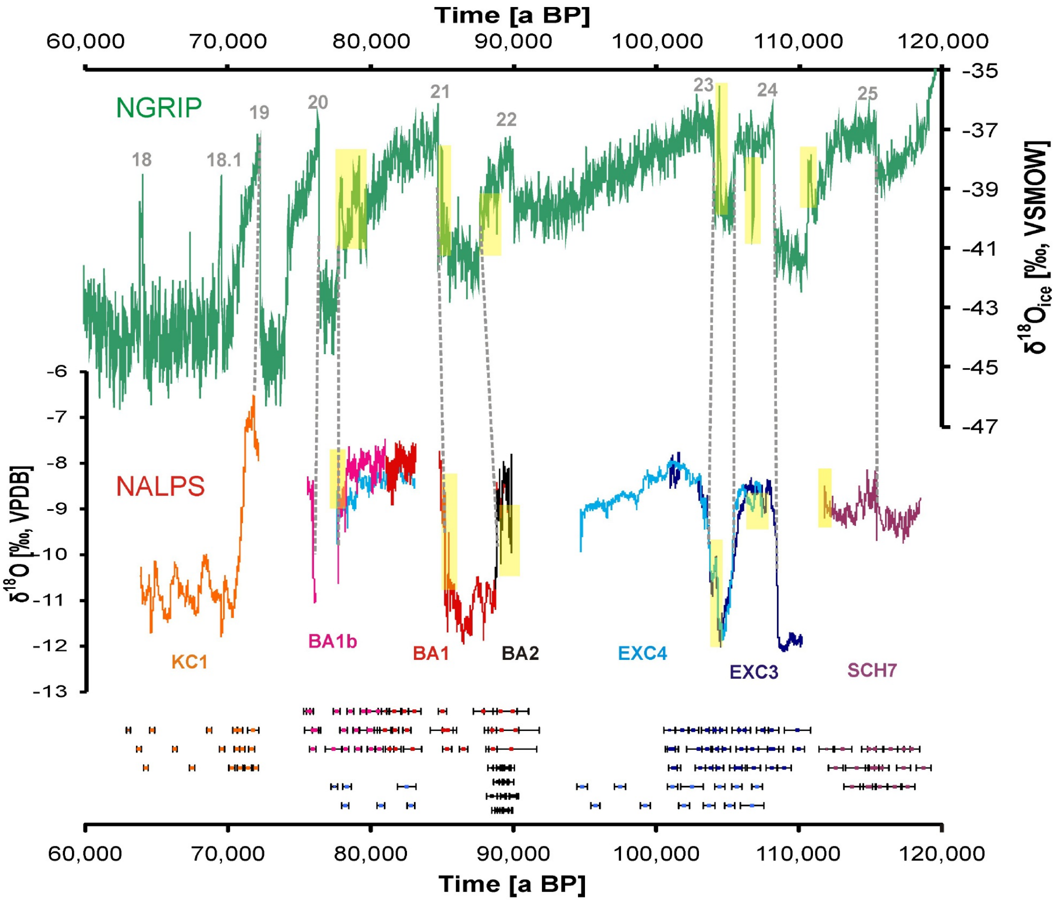

Figure 1.11: Comparison between the NALPS record and NGRIP (GICC05modelext timescale). The former consists of seven different stalagmites, plotted with different colors, and covers the time interval 60-120 kyr BP. The horizontal error bars on the bottom represent the uncertainties related to the U-Th dating method,while the yellow areas highlight sub-Dansgaard-Oeschger warming and cooling events.

Chapter 2

Timescales

In order to fully understand and correctly interpret ice core records and many other palaeoclimatic records, accurate timescales are necessary. First we need to relate measured data to time, to reconstruct the climatic history of a certain site or region. Once we obtain the best possible chronology, we can compare it with other available independent timescales, revealing possible discrepancies or agreement between them within the respective uncertainties. This is the way we have to follow to improve our knowledge about such a complex system as the climate system, analyzing its history and modeling its possible future evolution.
There are several available techniques for ice core dating, which range from annual layer counting to ice-flow models, radioactive dating and synchronization based on well-known age horizons (as volcanic eruptions for example), just to mention the main ones. Among them annual layer counting is definitely a landmark and also the one playing a central role in this work. We will also see how important synchronization of ice cores is, in the building process of a reliable timescale.

We are primarily interested in the Greenland NGRIP ice core and in the available chronologies used to date this core. Firstly, we will introduce a model-based timescale, called ss09sea, which has been initially used to date the GRIP[1] ice core. Secondly, we will describe the step-by-step construction of GICC05, a layer-

[1] Greenland Ice Core Project, achieved between year 1989 and 1992 in Central Greenland (see fig. 2.1).

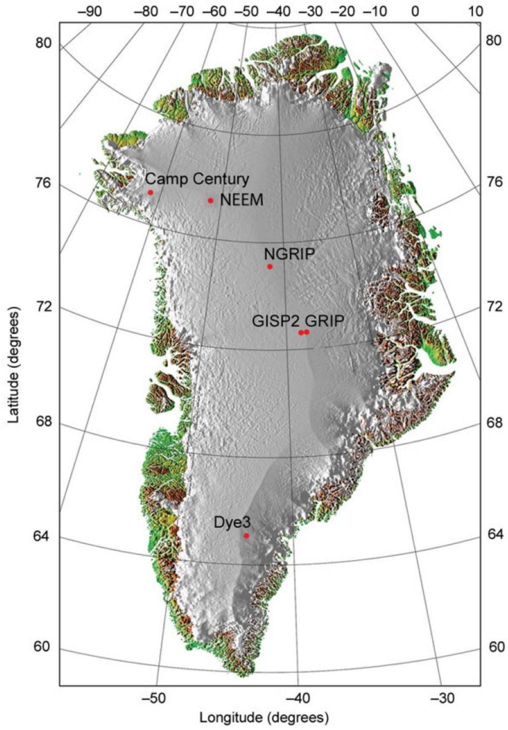

Figure 2.1: Map of Greenland, showing the locations of the deep ice core drilling sites [NGRIP-members et al., 2004].

counted chronology based on data provided by three different ice cores - DYE-3[2], GRIP and NGRIP - and extending back to 60 kyr b2k. Finally we will splice the GICC05 chronology and the model timescale at 60 kyr b2k, to obtain a unique timescale called GICC05modelext.

2.1 A model-based timescale: ss09sea

As already mentioned, the ss09sea timescale [Johnsen et al., 2001], preceded by ss09, arises as a chronology for the GRIP ice core, with the aim of dating the last glacial period forth to the transition into Holocene [Southon, 2004]. Though it is not a layer-counted timescale, counting data take part in its construction, as they

[2] Drilling terminated in 1981, in Southern Greenland (see fig. 2.1), DYE-3 was the first scientifically motivated ice core project.

set a constraint for the model. ss09sea is a glaciological model, which consists of two main parts. The first part is an ice-flow model [Johnsen et al., 1992] which gives an estimation of the layers thinning throughout the ice section. It is a simple model, called Kink Model, which assumes constant horizontal velocity of the ice down to a certain depth y_0, and then decreases linearly until it becomes zero at the bottom (see fig. 2.2 right), where no basal melting is considered to take place. The

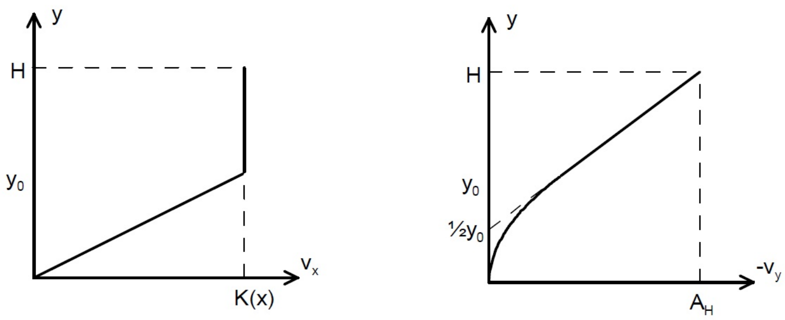

Figure 2.2: Horizontal and vertical velocity profiles, $v_x(y)$ and $v_y(y)$, as assumed in the Kink Model for the ice flow used to construct the timescale ss09sea [Centre for Ice and Climate]. H is the ice thickness, y_0 the kink depth and A_H the annual accumulation.

vertical velocity profile is derived from that horizontal, applying the continuity law, hence obtaining a vertical velocity decreasing with depth linearly until y_0, and then falling down to zero at the bottom. The dashed line (fig. 2.2) refers to the case in which basal melting occurs, and, therefore, the vertical velocity at the bottom is not zero. We just notice that the vertical velocity, $v_y(y)$, represents exactly the annual layer thickness along the depth. The reason for the choice of $v_x(y)$ is that the lower ice, close to the bedrock, is known to be warmer due to geothermal heat, and, thus, softer and deformable (velocity depending on depth). The second part is an accumulation model, based on the assumption of a relationship between the surface accumulation rate λ (expressed in meters of ice per year) and the δ^{18}O record provided by GRIP. This relationship [Johnsen et al., 1995] is:

$$\lambda(\delta) = 0.23\ exp(-10.09 - 0.653\delta - 0.01042\delta^2)\ m/yr \tag{2.1}$$

For NGRIP the coefficients have to be adjusted and the basal melting is taken

into account, but the essence of the relationship is exactly the same.
In the building process of an ice core chronology, the poor knowledge of past accumulation rates introduces the largest uncertainties, together with that of other parameters, such as basal melting, basal sliding and upstream effects [Schwander et al., 2001].
The obtained model was then constrained by two tiepoints. The two chosen events are the end of the Younger Dryas, dated 11.500 yr BP (before 1950 AD) counting data of the GRIP and the DYE-3 cores, and the onset of Isotope Stage 5d, at 110 kyr using the SPECMAP timescale [Martinson et al., 1987]. A third tiepoint is added, which corresponds to the so-called 8.2 kyr-event, a cold event occurred 8170 yr BP. In the Holocene we find that this model and the counting provide ages in agreement within a few decades, i.e. within the uncertainties [Southon, 2004]. That is a good result for a pure model chronology, but we still have to consider its limits. Compared to the previous model ss09, the ss09sea model includes a correction of the δ^{18}O-accumulation relationship, which takes into account past changes of seawater δ^{18}O caused by changes in global ice volume. But there are also other possible sources of variability for δ^{18}O, related to the limited knowledge we have about circulation in the atmosphere and in the ocean during glacial time, sources which are not considered in the model. For example, variations in time of the location of the moisture source regions for Greenland precipitation [Masson-Delmotte et al., 2005], changes in the conditions along the transport path [Charles et al., 1994] or the existence of other large ice sheets are not taken into account.

2.2 A layer counted chronology: GICC05

2.2.1 Dating methods: layer counting

Annual layer counting is essentially based on the fact that certain substances contained in ice or physical properties of it show a seasonal signal along the span of an year. It means that, for example, their concentrations or values are different in the winter and in the summer (as is the case for δ^{18}O), or they present a specific behavior corresponding to a certain time of the year, as for instance dust, that shows a stronger concentration peak in the winter-spring period (see section 1.1.3). These amplitude differences of the signals can be related to several causes and parameters, such as changes in temperature (as explained for the case of δ^{18}O in the section 1.1.1), insolation variability, atmospheric circulation and so forth. The existence of annual layers and the way they are built up was already introduced in the section 1.1.3. Here we want to summarize the main features of annual layers, which are important for our measurements and will affect their resolution and quality. Annual layer thickness obviously depends in the first instance on the mean accumulation rate at a specific drilling site. A low accumulation rate could produce layers whose thickness is too small to be resolved. Once snow has been deposited, the new layer might still become subject to mixing and re-deposition caused by wind, but this seems to be of minor concern at NGRIP. Instead, other processes, such as diffusion and chemical reactions, represent crucial factors affecting the seasonal signal we are interested in. In the upper part of the ice core, constituted by porous firn, a smoothing of the isotope seasonal signal takes place in the deposited layers, mainly due to diffusion of water and air circulation (see section 1.1.2). Deeper in the core, where firn becomes ice, diffusion effects are much smaller, as the molecules capacity to move decreases sensibly. Diffusion affects primarily water isotopes, as impurities and trace elements are usually constituted by larger particles, especially dust, which cannot move easily in ice. Deconvolution techniques are sometimes used to remove the effects of diffusion from the isotope record.

Other factors which can contribute to annual layers obliteration are related to the ice-flow dynamics and to the thinning of the layers with depth. Difficulties in identifying annual layers in deep ice can arise from the significant compressive stresses acting vertically but also laterally on ice, especially if the stress rate of "clean" layers (usually corresponding to warm periods, thus containing small quantities of dust) and "dirty" layers (cold periods, rich in dust) are different. Hence we could find layers that are tilted from the horizontal plane or merged together and thus cannot be distinguished. this is the so-called microfolding and an example is given in fig. 2.3. Folding of the bottom part of the ice can occur due to a particular bedrock morphology. Therefore an ice core is a local picture of the vertical stratig-

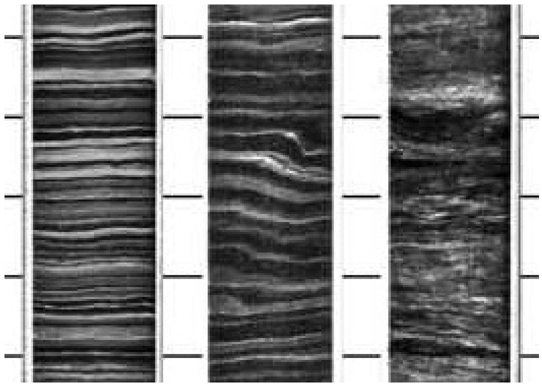

Figure 2.3: These theree different ice sections from NGRIP (modified from [Svensson et al., 2005]) show very thin but regular annual layers (left), microfolding (center) and hardly distinguishable layers (right).

raphy of a glacier, which could be different just a few meters apart, and which contains a theoretically complete climatic chronology of that particular site. In particular each section of the core reports a piece of history of the ice coming from upstream along the flowline passing at that point. For this reason, for the last drilling projects in Greenland, sites close to the ice divide have been chosen, in order to limit as much as possible deformation disturbances of the layer structure due to the ice-flow.

2.2.2 Building the timescale

The Greenland Ice Core Chronology 2005 (GICC05) is a stratigraphic timescale based mostly on the NGRIP ice core [[Rasmussen et al., 2006, Vinther et al., 2006, Andersen et al., 2006, Svensson et al., 2006, 2008]. It is interesting for us to summarize the building process of this chronology, at least for two reasons. First because GICC05 represents a reference chronology for the NGRIP ice core, and, secondly, because we can have an overview on how the layer counting process concretely takes place, with its limits and uncertainties.
Reaching back to 60 kyr b2k, this chronology has been achieved in a series of stages, matching several kinds of stratigraphic data from three different ice cores - DYE-3,

GRIP and NGRIP - and has become the current reference timescale for Greenland. The basic idea lying behind this chronology is that of dating ice by annual layer counting, continuously from present time back into last Glacial, where possible, and then to match timescales of different cores using volcanic layers or other common age horizons, such as geomagnetic events, Dansgaard-Oeschger events, etc. The availability of new high-resolution Continuous Flow Analysis (CFA) impurity records from the NGRIP ice core was a major prerequisite for developing this new chronology.
Figure 2.4 gives an overview of how the GICC05 chronology was made, with the contributions of the three mentioned cores.

The youngest section of the GICC05 chronology, from present back to 7.9 kyr

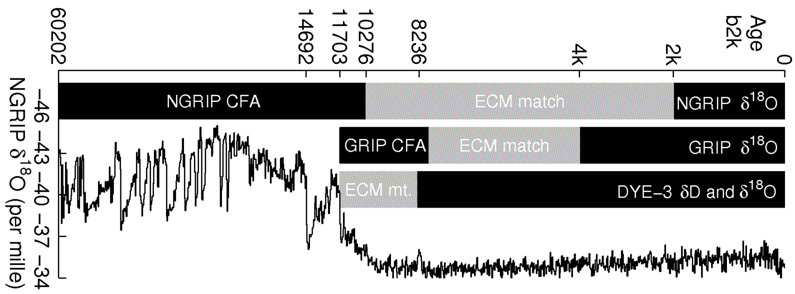

Figure 2.4: The GICC05 chronology is built with the contributions of three different ice cores - DYE-3, GRIP and NGRIP - and their multi-parameter records. All the available records are used, and here time intervals are shown, where different records overlap or are matched using ECM reference horizons, thus ensuring consistency between them [Centre for Ice and Climate]. The chronology has then been extended from present time back to 60 kyr b2k.

b2k, is based on the DYE-3, GRIP and NGRIP stable isotope records. Mainly the DYE-3 stable isotope record is used, as it is considered as the best available Holocene record in Greenland [Hammer et al., 1997], because of the especially high accumulation rate of the drilling site. Thanks to the small diffusion effects this $\delta^{18}O$ record enables us to detect annual layers clearly. The chronology has then been extended down to 11.7 kyr [Vinther et al., 2006] - thus covering the entire Holocene period - basing on the GRIP CFA data, matched with the DYE-3 and the NGRIP cores using volcanic reference horizons in electrical conductivity.

The matching process is achieved counting annual layers in the time intervals included between ECM volcanic horizons for each ice core, and then comparing these independent results and deciding if possible discrepancies between them can be resolved. In the end the best number of years is chosen for each interval, consistently with all the used data, and imposed to all the cores [Vinther et al., 2006].

The second stage of the creation of GICC05 was the achievement of a synchronized timescale covering the interval 7.9-14.8 kyr BP Rasmussen et al. [2006], where multi-parameter data from GRIP and NGRIP were used (see fig. 2.5 for an example). The choice of basing the identification of annual layers on more data series, if they are available and present with sufficient resolution, improves the quality of the timescale, especially when multiple annual spikes are present in some parameters Rasmussen et al. [2006]. For NGRIP, concentration records of several soluble ions were used, such as NH_4^+, Ca^{2+}, and the meltwater conductivity series as well. Then dust data and ECM profiles were used, and also the visual stratigraphy (VS), whose profile was smoothed by applying a Gaussian filter, because of the presence of many close, thin layers representing sub-annual variations Rasmussen et al. [2006]. ECM, $[NH_4^+]$, $[H_2O_2]$ and $[Ca^{2+}]$ from GRIP core were used. The datum of this section of the scale is the volcanic horizon recoverable during the 8.2 kyr cold event, dated in the DYE-3 ice core to 8236 $\pm$ 47 yr b2k [Vinther et al., 2006]. The uncertainty which affects the dating - here 47 years - is called maximum counting error (MCE) and we will explain its meaning below.
Moving back into last glacial period, annual layers become thinner and only the NGRIP ice core is able to provide a well-resolved annual signal. As mentioned in section 1.2, the reason for the relatively thick annual layers in NGRIP glacial ice is the basal melting of the ice sheet at this site, which enables the layers thicknesses to remain around an average of 7 mm ice yr^{-1} along the entire lower section of the core [NGRIP-members et al., 2004]. Hence layer counting in the following two sections of the chronology, the glacial sections 14.8-41.8 kyr b2k [Andersen et al., 2006] and 41.8-60 kyr b2k [Svensson et al., 2008], is solely performed on NGRIP data. In the former section (14.8-41.8 b2k) CFA-measured concentrations of Ca^{2+}, Na^+, NH_4^+, SO_4^{2-} and NO_3^- were used, as well as ECM and VS (visual stratig-

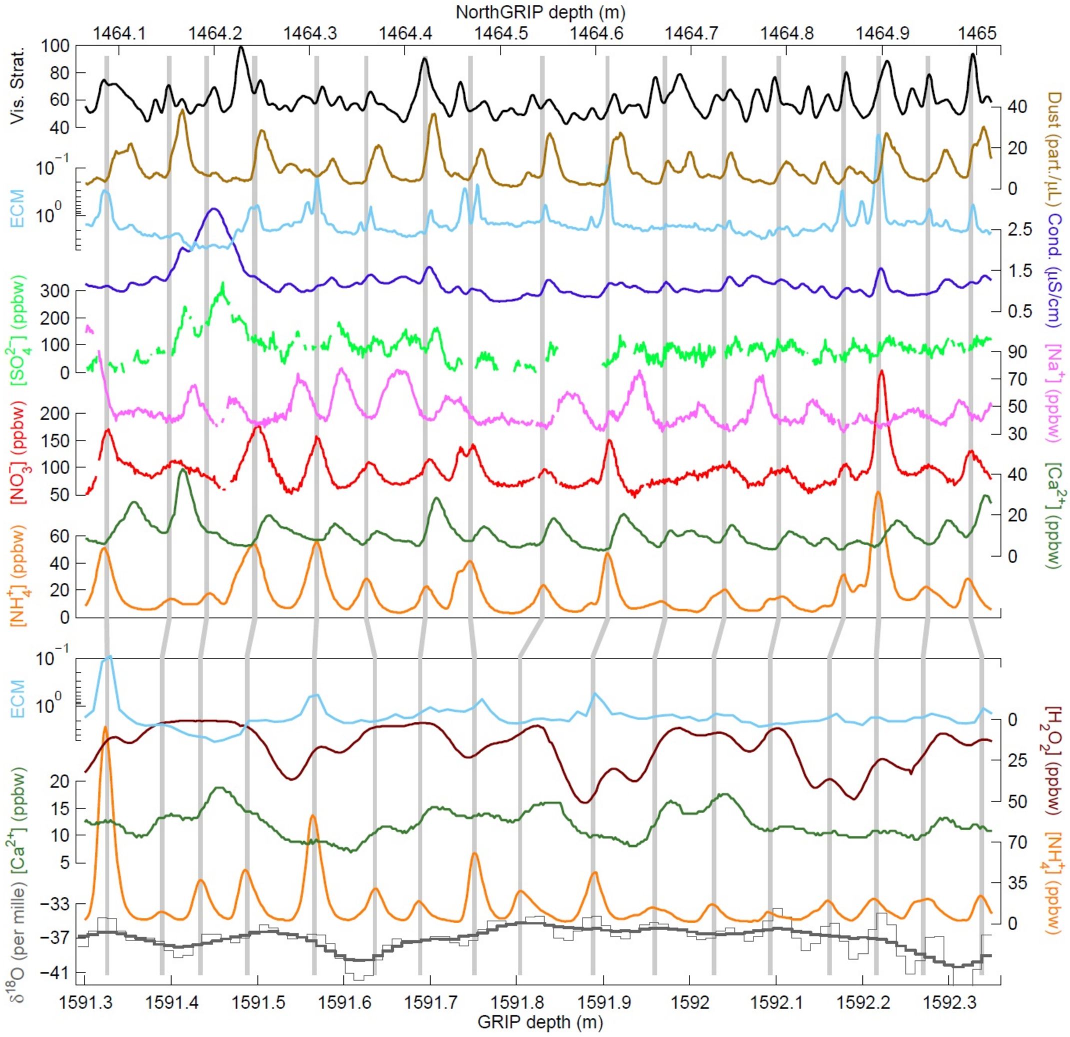

Figure 2.5: Example of layer counting performed on an early Holocene section of NGRIP (upper nine records) and GRIP (lower five records) ice. The gray vertical bars show the annual layers, that here are marked at summer peaks [Rasmussen et al., 2006].

raphy) records. In the latter (41.8-60 b2k) the same data are available, whereas for the stadials only high-resolution records can resolve thicknesses of about 1-1.5 cm, namely conductivity, ECM and VS.
Such a constructed timescale can eventually be extended further back in time, using the ss09sea model. As we will see in section 2.2.4, the two timescales show a reasonable agreement throughout all of the considered period, showing an estimated offset of 705 years at 60 kyr b2k. Thus, Wolff et al. [2010] chose to splice the two timescales together at 60 kyr, simply shifting the ss09sea ages older than 60 kyr by 705 years.

2.2.3 Errors and uncertainties

Now that the chronology is done, we spend a few words about the sources of errors in the counting process and the corresponding uncertainties. Sources of errors, which we already mentioned, are imperfections and deformation effects in the stratigraphic structure of the core, as, for example, tilted layers, folding in the bottom of the core or even missing layers due to extremely low accumulation rates. We also have to mention the presence in all cores of the so-called brittle zone, usually located between 800-1200 m depth, which is particularly fragile. This can cause fractures in ice and some small sections of ice could be lost or not worth for analysis. Fortunately this fragile section occurs at different depth intervals for the three cores involved here. Then parts of the core might get lost during the drilling and the handling stages, but usually these cases are at least reported and well-known. Further errors are introduced while sampling and analyzing the cores, and sometimes the resolution of the measuring devices is too low to detect all the variability of the ice, leading to a loss of information.
Vinther et al. [2006], Rasmussen et al. [2006], Andersen et al. [2006], Svensson et al. [2008] show that all the uncertainties mentioned so far are eventually negligible, if compared to the interpretation errors, leaving to the latter a major role in evaluating the overall uncertainties.
As the data need to be interpreted, in order to become a numeric result in terms of time, we have to quantify the uncertainty corresponding to the data interpretation.

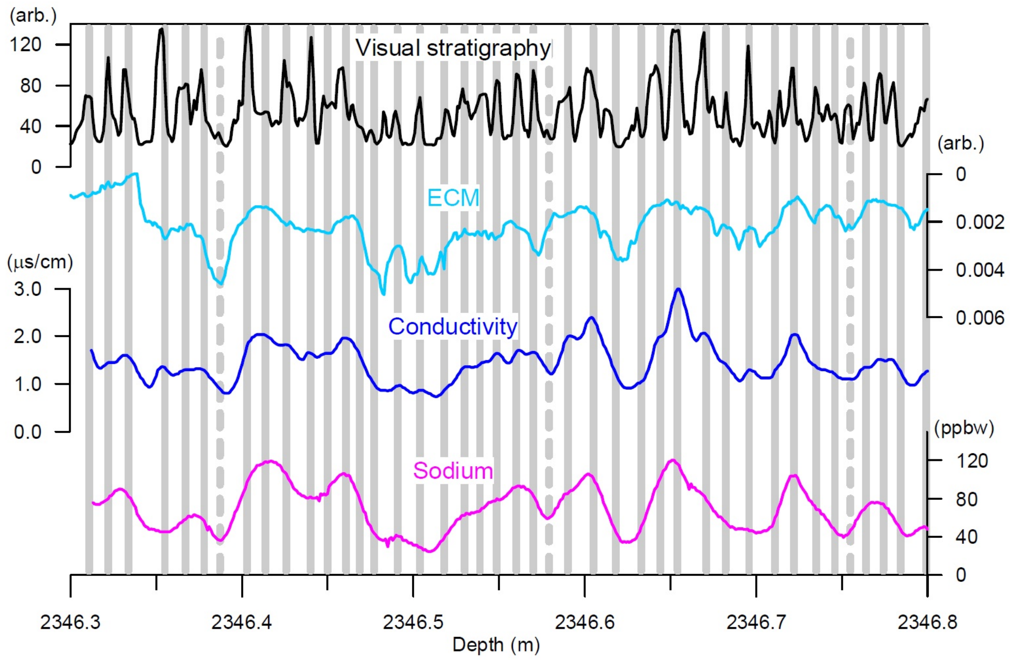

Figure 2.6: Example of annual layer counting during a Stadial. Certain/uncertain years are indicated by gray/dashed vertical bars. Here visual stratigraphy and ECM have the best resolution [Svensson et al., 2008].

First we will briefly go through the counting procedure.

For the counting, all the available records, which show a sufficiently resolved signal in the analyzed section, are visualized on screen (fig. 2.6), and the investigator will place marks at those peaks, that are considered likely to be years. In that, he takes into account several factors. First of all, the possible presence or not of the same peak in several or even all the available records. Then the possible shifts have to be considered, between peaks of different species, if they peak at different times of the year (e.g. spring for dust and summer for NH_4^+). If a peak is recognized as a certain year (more than 75% of probability), then a black dot is placed and the total amount of years increases by one unit. A year can also be counted as uncertain (probability between 25% and 75%), in that a white dot is placed, which counts as 0.5 ± 0.5 years Rasmussen et al. [2006]. This happens if the peak is not found in most of the records, if the shift between different records cannot be interpreted as seasonal or if a certain feature in the data, as for example a shoulder close to a larger peak cannot be counted as a peak with more than 75% of confidence. Hence, an estimation of the counting uncertainty, i.e. the data interpretation error, is introduced, which is called Maximum Counting Error (MCE). For n uncertain layers the MCE is given by $n \times 0.5$ years. The MCE, as it is estimated here, can be regarded as very conservative, since it is obtained by linear error accumulation [Andersen et al., 2006]. As mentioned above, the MCE represents the dominant part of the total uncertainty, but it does not account for a possible bias, which could affect the annual layer identification process Rasmussen et al. [2006].

In order to reduce the uncertainty, the counting is performed by several (usually 2 or 3) different independent investigators. Each of them provides an annual layer profile by identifying certain and uncertain years. Then, the different profiles are compared, and each point where they disagree is discussed with a further independent investigator (arbitrator). When possible, an agreement is reached and the final counting is provided Rasmussen et al. [2006].

2.2.4 Results and comparison with other timescales and reference horizons

The first result, which this chronology carries with itself, is the close correspondence between annual layer thickness and climate, i.e. the stable isotope record (δ^{18}O) shown in fig. 2.7. This agreement holds to first order for the whole 60 kyr period. For the glacial period we can see that layer thicknesses are around 1-2 cm in cold periods, and increase up to 2-3 cm in milder times [Andersen et al., 2006, Svensson et al., 2008]. In addition, in the late Holocene and in climatically stable periods of the last glacial termination, the layer thickness turns out to be approximately log-normally distributed (fig. 2.8), in accordance with the assumption that accumulation is the sum of independent precipitation events [Andersen et al., 2006]. In fig. 2.9 the comparison between the GICC05 time scale and other independently dated records is shown. The differences between GICC05 and the other timescales are plotted in different colors, while the gray shaded area represents the GICC05 MCE, i.e. the counting uncertainty, almost linearly increasing when we

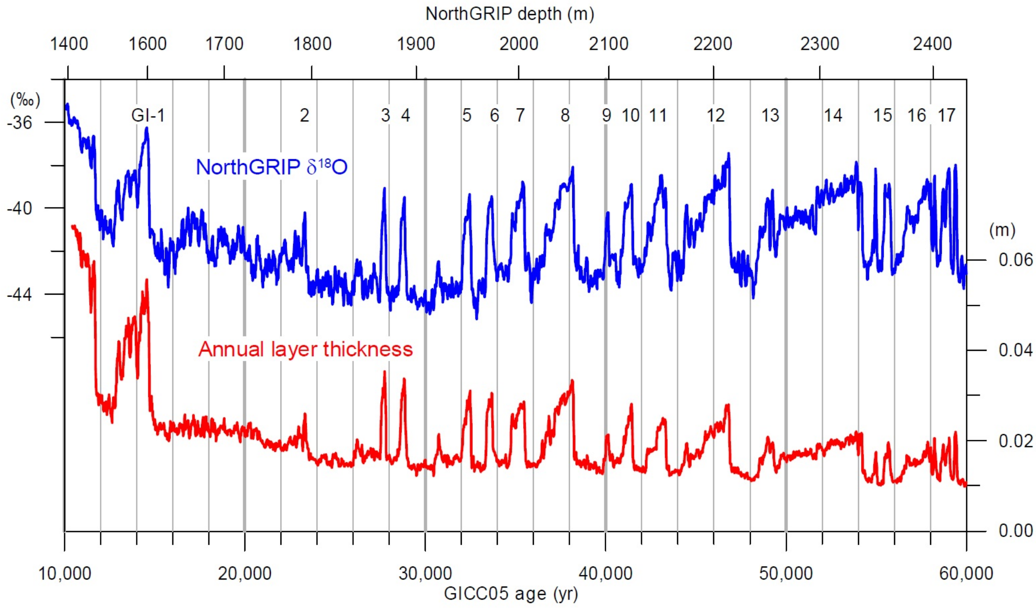

Figure 2.7: NGRIP $\delta^{18}O$ and annual layer thickness profiles according to GICC05 [Svensson et al., 2008].

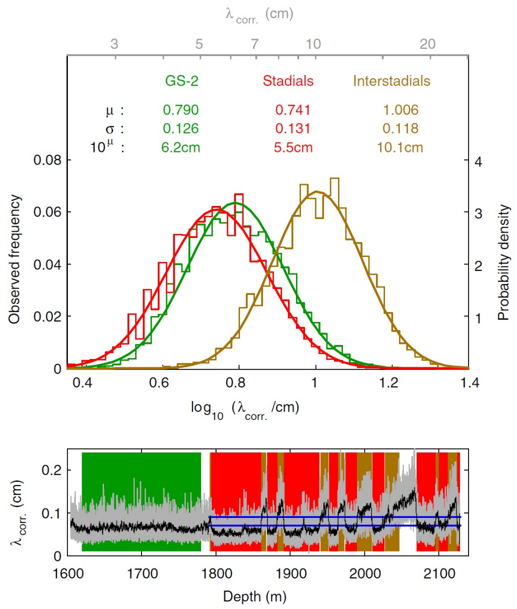

Figure 2.8: Distribution of annual layer thicknesses ($\lambda_{corr.}$ is the strain corrected thickness) for Stadials (red), Interstadials (yellow) and for the cold GS 2 period [Andersen et al., 2006].

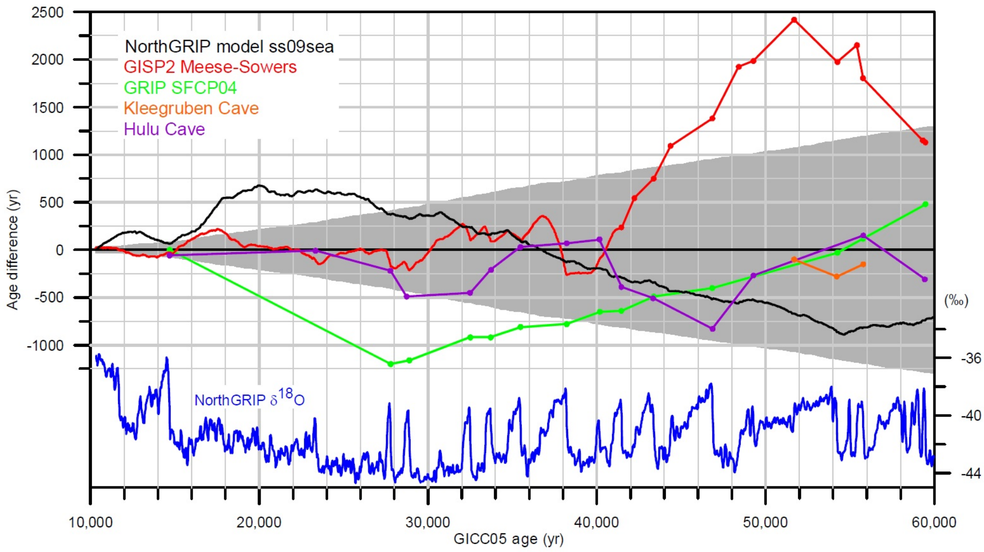

Figure 2.9: Comparison between the GICC05 time scale and other independently dated records. The differences between GICC05 and the other timescales are plotted in different colors, while the gray shaded area represents the GICC05 MCE, i.e. the counting uncertainty [Svensson et al., 2008].

move back in time. We see that there is an overall agreement between the GICC05 and the ss09sea timescales (black line in fig. 2.9) throughout the 60 kyr, with age differences up to 900 yr. Hence, GICC05 suggests that the assumed relationship between the δ^{18}O and the accumulation rate is reasonable. Nevertheless, the two timescales show a larger discrepancy in the 15-18 kyr period (corresponding to MIS2[3]), where GICC05 suggests thinner layers, thus counting around 500 more years than the model. It could mean that the above-mentioned relationship is not valid in this time interval. Beyond 18 kyr a gradual opposite effect is observed, as GICC05 reveals slightly thicker layers than the model, suggesting that the model could need a different tuning [Svensson et al., 2006, 2008]. Another comparison is made with the GISP2 record, showing a quite good agreement between the two records back to 40 kyr b2k. However, the older part of the record shows increasing discrepancies between them of up to 2.4 kyr.

[3] Marine Isotope Stage 2.

Chapter 3

Experimental setup

3.1 Continuous Flow Analysis (CFA)

The CFA-setup developed at the Center for Ice and Climate of the University of Copenhagen, used to make all the measurements applied in this work, is shown in fig. 3.1. The main characteristic of this setup is its capacity to resolve very thin ice layers down to a thickness of less than 10 mm[1]. Such a high resolution is obtained by running the system at low melt speed and by minimizing mixing volumes in the most critical sections of the setup, i.e. the melthead and the debubbler, which we will shortly describe. This high resolution allowed us to achieve the first layer counting on such an old and deep ice section, which has not been done before. The choice of a low melt speed enhances the resolution but also restricts the number of different species we are able to analyze simultaneously. Our measurements thus focus on only four parameters, which we will present soon. Other CFA-setups, instead, focus on measuring many parameters simultaneously, as, for example, the CFA in Bern [Röthlisberger et al., 2000, Bigler et al., 2007, Kaufmann et al., 2008], which measured TAC[2], dust, $[Na^+]$, $[Ca^{2+}]$, $[NH_4^+]$, $[NO_3^-]$, $[SO_4^{2-}]$, $[H_2O_2]$, $[HCHO]$ and the electrolytical conductivity on a section of NGRIP [Kaufmann

[1] Based on standard measurements and the comparison between Holocene and Glacial sections of the ice, a depth resolution of only a few millimeters was achieved [Bigler et al., 2011].

[2] Total air content.

et al., 2008].

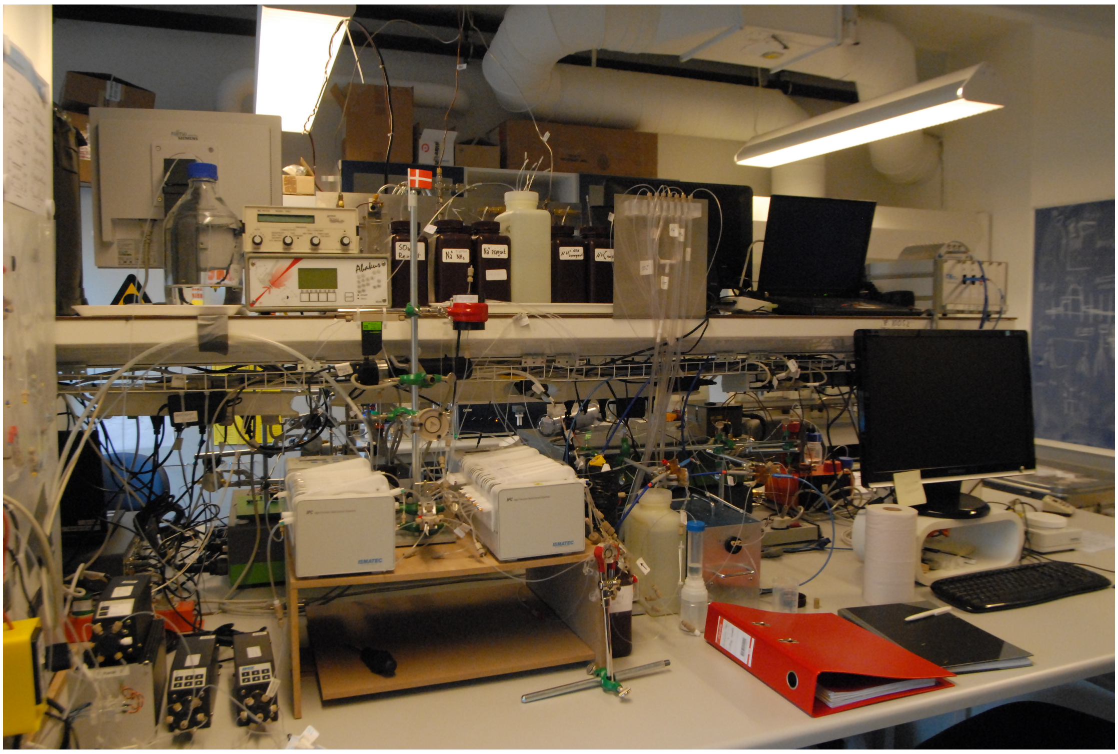

Figure 3.1: The CFA-setup at the Centre for Ice and Climate, Copenhagen.

In fig. 3.2 we show a little sequence of our data, plotted together with the corresponding Bern-CFA measured sequence [Ruth et al., 2003, Bigler et al., 2011], to see the different spatial (and, thus, also temporal) resolution of the two systems.

Following the layout in fig. 3.3, we start from the left top with the freezer, which contains the melthead, which is maintained at a temperature of $-20\,^{\circ}\mathrm{C}$. The ice samples are kept in plexiglass holders, which are then placed on the melthead (having a temperature of $30\,^{\circ}\mathrm{C}$) and assist the melting process by guiding the ice core and holding it in a constantly vertical position. Another fundamental aspect of these holders is the presence of a steel-PTFE weight on top of the melting sample, connected to an encoding device by a wire, and providing the melting speed of the sample (registering its position). Each holder is designed in order to fit exactly with the shape of the melthead, which consists of a surface with a 2-mm-high ridge delimiting inner and outer collection areas. This particular ridge

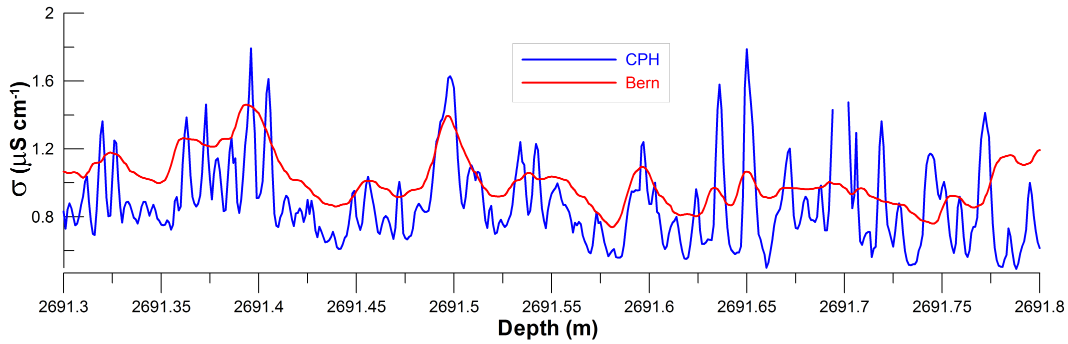

Figure 3.2: Here we see a small section of NGRIP ice from a depth of about 2691.5 m, during the cold period called GS 22. The meltwater conductivity is shown, using the red line to represent the Bern-CFA data [Ruth et al., 2003, Bigler et al., 2011], and the blue one for our measurements, achieved with the CFA-setup in Copenhagen. The difference in resolution is easily recognizable since the Bern signal is much smoother than ours.

keeps the separation between the clean meltwater from the inner section of the core, and the contaminated outer part (see fig. 3.4). Also thanks to an overflow of around 10%, directed from the inner to the outer area, we are able to keep the clean sample from being contaminated. The meltwater coming from the outer section of the core is collected and driven directly to waste, while the clean water flows through a tube towards the detecting devices. Along its path, the sample encounters two automated injection valves, which allow the user to switch between different sources as for instance the sample itself, a bottle of standard blank water, called mQ water[3], or other standard solutions, which have been prepared before starting the measurements in order to calibrate the setup. After the valves, there is a bubble detector that warns us with an acoustic signal when the meltwater is not flowing continuously or it contains too much gas, which could represent a problem for the detectors or for particular elements of the setup. In order to remove this gas, right after the bubble detector is placed a debubbler: it is a device that should ensure the removal of almost all the air bubbles. As can be seen in

[3] mQ water is purified water thus presenting concentrations of TOC (total organic carbon), minerals and substances of interest in our analysis close to zero.

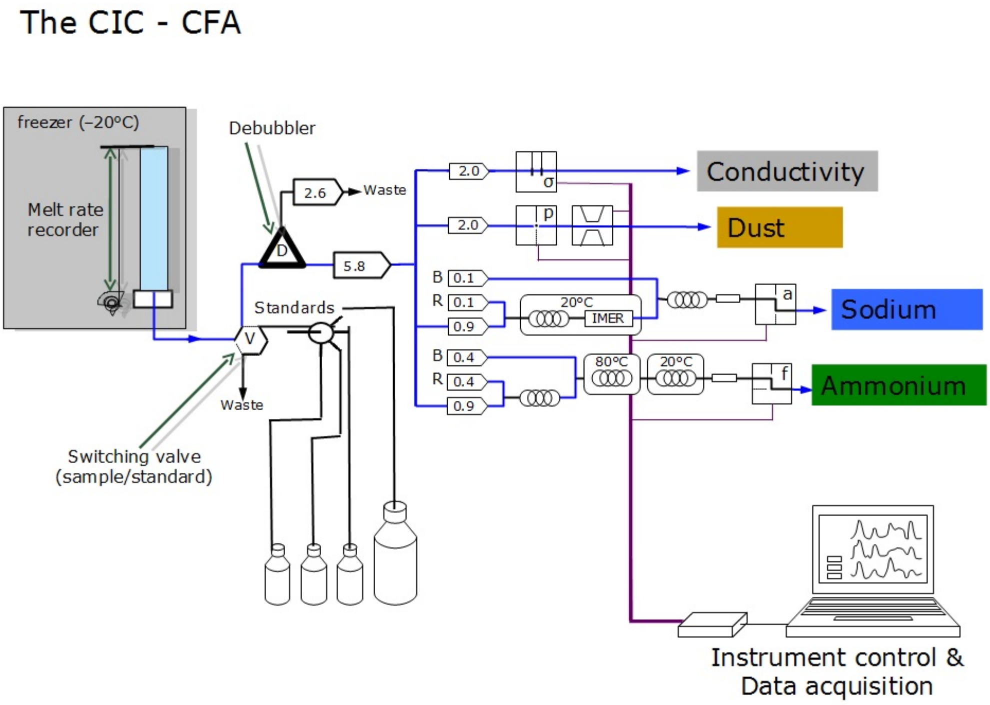

Figure 3.3: Schematic of the CFA-setup

fig. 3.5, it has a flat, triangular shape with three holes, one inlet and two outlets. Because it is lighter, air tends to flow upwards and to exit the triangular structure from the upper hole, together with a small excess of meltwater. This way the air is collected and sent to other instruments assigned to specific gas measurements (e.g. methane concentration) or just to waste.

After the debubbler, the sample is finally pushed in four different channels leading to the same number of detecting units, where we measure dust particles, conductivity, sodium concentration ($[Na^+]$) and ammonium concentration ($[NH_4^+]$). The pressure needed to push the liquid through the system is provided by a peristaltic pump and the flow rate of each line is chosen by tubings of specific diameters (identified by numbers in fig. 3.3).

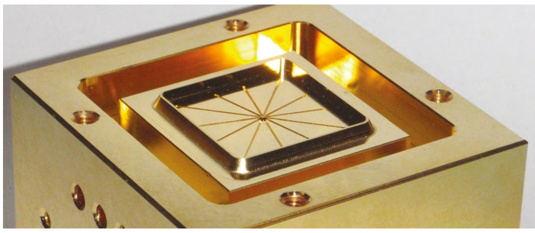

Figure 3.4: The melthead with its 2-mm-high ridge dividing the melt surface into two distinct areas [Bigler et al., 2011].

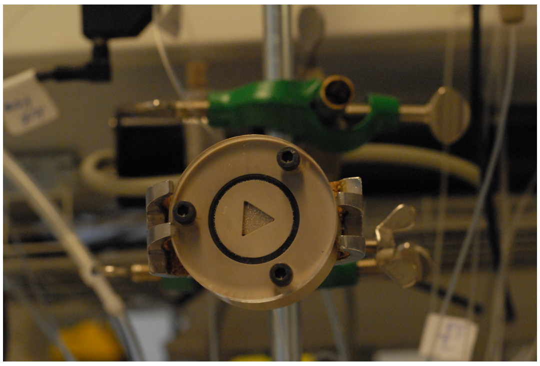

Figure 3.5: The debubbler.

3.1.1 Dust

The dust line consists of a particle detector (Abakus with LDS 23/25bs sensor, Klotz). The counting takes place in a flow cell where a laser beam is produced. When the sample flows through this cell, it causes the attenuation of the beam that gives us a measure of the particle size. This way we are detecting only the insoluble fraction of dust. The calibration of the particle detector is achieved using a flow meter.

3.1.2 Conductivity

The electrical conductivity of our sample is measured by a conductivity meter using a micro flow cell (3082 with micro flow cell 829, Amber Science). This device provides a measure of the total amount of free ions (positive and negative) present in our sample [Kaufmann et al., 2008].

3.1.3 Sodium

Absorption spectroscopy is used to detect sodium in our sample. According to the scheme of fig. 3.3 (right side of the figure), first a sodium reagent is added to the sample. In order to mix them properly we let them flow through a coil in a turbulent regime. Subsequently the fluid encounters an IMER-column (where IMER stands for IMmobilized Enzyme Reactor) which enhances the sodium signal considerably, making it detectable for us. After crossing the IMER, the sample is mixed with a buffer containing a 17mM (mM: milliMolar, it gives the concentration) ammonia solution that keeps the pH constant. Again a coiled tubing is used to mix the two fluids which cross an accurel (a microporous polypropylene membrane tubing) removing the air bubbles that the debubbler was not able to get rid of.

Afterwards, the sample, mixed with the reagent and the buffer, reaches the detecting unit, which consists of a flow cell (with the shape showed in fig. 3.6) that presents a linear path crossed by a light beam[4] that is then absorbed more or less depending by how much sodium is found in the fluid. The less light we measure, the more sodium there is in the sample that has absorbed the light. This provides a direct measure of sodium concentration[5]. The way light is absorbed can be described by an exponential law that contains two parameters. In order to assign to these parameters a number, we first need to calibrate the system, which means that we have to run a certain number of standards[6] that informs us about how the system reacts to well-known concentrations of the substance we detect afterwards.

[4] We used the deuterium halogen light source DT-Mini-2-GS, Ocean Optics [Bigler et al., 2011]

[5] In details, the photometric determination of sodium is based on the absorbance of o-nitrophenol produced by hydrolysis of o-nitrophenyl-β-D-galactopyranoside (ONPG) catalyzed by beta-galactosidase. Since the enzyme activity depends on the sodium concentration in the medium, the sodium concentration can be determined by monitoring the o-nitrophenol concentration [Röthlisberger et al., 2000].

[6] A standard solution is a solution of a certain substance of interest mixed with water at a specific and well-known concentration. We used three different standards for sodium and we run a calibration before and after each measurement.

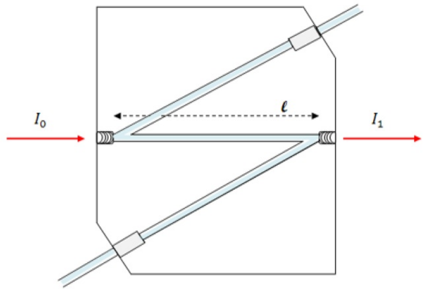

Figure 3.6: The flow cell where sodium is detected (from [Nielsen, 2009]).

We will see more about these calibration coefficients later in section 4.3. This measure is affected by different factors such as for example the temperature (the whole sodium line works at room temperature), the flow rate and the integration time of our spectrometer[7] (USB2000, Ocean Optics [Bigler et al., 2011]).

3.1.4 Ammonium

A fluorescence method is used to detect ammonium [Röthlisberger et al., 2000, Bigler et al., 2011]. As for sodium we can follow the scheme in fig. 3.3. At first a reagent, called OPA (o-phthaldialdehyde), is added to the sample and mixed with it using a coil. Subsequently also a buffer is added, in order to improve sensitivity, and afterwards the whole mixture flows through another coil immersed in a water bath at a temperature of 80 °C, needed for the reaction to be accelerated. Before the detecting unit an accurel is placed to eliminate the last air bubbles that could stick inside the flow cell, blocking the flow and affecting the values of measured fluorescence. Then the sample enters the flow cell, through which an LED can emit light. The LED light excites the entering molecules that absorb a photon. Then the excited molecules react by emitting another photon of different energy and,

[7] The measured value of absorbance has to be saved and stored before the next measure can be done. Thus only a fraction of time, for example one second of activity, is actually used to make the measurement, and this value has to be chosen accurately in order to have the instrument ready again in a reasonable time, but avoiding the loss of too much sample during the not-measuring time. The integration time we set for sodium ranges from 150 to 300 milliseconds.

thus, different wavelength, which we detect using a photomultiplier. A calibration is needed also for ammonium which we repeat before and after every measurement. The law, which relates the emitted light intensity and the concentration, is linear and requires the knowledge of one coefficient besides the baseline value, measured by running the blank (mQ water) through the system.

Chapter 4

Measurements and results

4.1 Sample preparation

Before we analyzed the samples a few steps were required to prepare the ice for the measurements.
First we checked all the needed samples and their availability in the freezer of the Centre for Ice and Climate. Among the required bags[1] - NGRIP bags from n.4872 to n.4963 - there were two entirely missing bags (n.4878 and n.4881) and a section of about 11 cm of bag n.4944 was missing too. For each core, stored in the freezer, first we had to find and register all the visible breaks or other issues affecting the core. Second we had to cut the core in order to obtain the 34mm×34mm square section used for our CFA measurements (fig. 4.1). The provided CFA-sample was then cleaned and put in a new numbered bag, ready for use. The whole handling of the samples had to take place inside the freezer, at a temperature of $-20\,°C$, to preserve the ice. All the samples have been prepared a few days before the measurements started and were stored in the freezer for the remaining time.

[1] The NGRIP ice core has been cut in 0.55 m long sections, called bags.

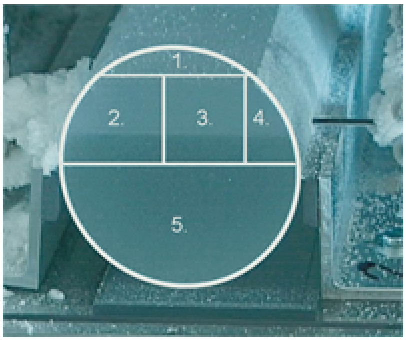

Figure 4.1: Each piece of the ice core section is used for a different goal: 1) physical properties of the ice; 2) gas; 3) CFA; 4) stable isotopes and 5) on this piece electrical conductivity is measured, and then a piece identical to number 3 is obtaind, which we used for our measurements. A part of the rest of piece 5 goes to the NGRIP Archive [Centre for Ice and Climate].

4.2 Calibration of the CFA system and measurements

Overall we had to analyze 90 bags and we decided to melt sequences of four bags continuously. This means that we could melt 2.2 meters of ice without stopping the measurements, which resulted in an effective improvement in terms of time. First, the system needs some time to get started, before measurements can be achieved, and thus we prepared the system just once every four bags; secondly, in the following processing stage the data handling could be done in a shorter time because only one file collected the data of four different bags. The continuous melting was achieved thanks to a special holder with a removable side, which enabled us to recharge the holder with the next core before the sampled one ended. With this method we were able to melt about 8-12 bags per day (4.4-6.6 m). As mentioned in sections 3.1.3 and 3.1.4, before we could melt and measure the ice samples, we had to calibrate our system for sodium and ammonium. Figure 4.2 shows an example of calibration for Sodium and Ammonium in which we can recognize the three sodium peaks and the two ammonium peaks, corresponding to different concentrations of these elements. As hinted in section 3.1, the calibration process consists in analyzing a series of standard solutions containing well-known concentrations of Sodium and Ammonium. We register the response of the system (i.e. the height of the peaks referred to the initial baseline) and then we use these values to obtain the coefficients we need to calibrate the final data. Calibrations represent a sort of reference system for further measurements, and, hence, they should be done regularly in time, to register any kind of variations in the system. Therefore, we decided to run a calibration before starting with our measurements, and then another one after each the four-bag sequence was analyzed. The melt rate

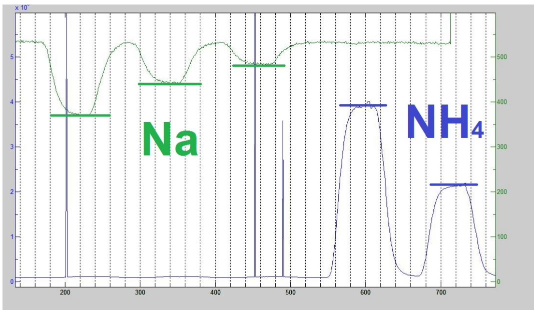

Figure 4.2: This figure is an example of sodium and ammonium calibration. We can see two peaks for the ammonium standards and three for sodium.

was kept at around 1.5 cm/minute throughout all the measurements. The required time to melt four bags was therefore about 2 h 30 min. Before each four-bags sequence, we melted 10 cm of mQ ice, which later could be easily distinguished from the sample to identify the precise start of the latter. Another reason to use this mQ ice was to avoid ice sample loss in case of possible issues/troubles right after the system had been started. During the melting sessions we met several difficulties, but, fortunately, all of them could be managed without any significant data loss. For example, the most frequent problems occurred at the debubbler stage, where air stuck, making it difficult for the sample to flow. Equally, sometimes air bubbles got stuck in the flow cell used to detect sodium. Large high concentrations of air usually occurred in correspondence to breaks in the ice or between one core and the next one. A few times we had to change all or part of the tubing in the system because they were old or broken. In one case we also tried to improve the quality of the sodium signal, changing the flow cell and the integration time of the detecting device without any major improvement.

4.3 Data processing

The whole CFA system is controlled from a computer terminal using LabVIEW, a graphical programming environment. LabVIEW is an interface that interacts with all the electronic components of the CFA system and enables us to control them by the terminal. It also shows our measurements in real time and saves all the data in files. Once the data are collected, we have to process them by going through several steps, which we will now look into.
First, we have to insert the exact dimensions of each core and the values of the coefficients we calculated for the sodium and the ammonium calibrations. Then we have to synchronize[2] the four collected signals (dust, conductivity, $[NH_4^+]$ and $[Na^+]$), which we achieve by visualizing them all together on the screen on a time scale and shifting them as much as needed relatively to each other. In addition the change from mQ water to the sample can be identified and used as time origin. In practice, we look at the first clear contamination peak that we can recognize at the beginning of each signal, and take this time as simultaneous for all the records. The reason why different channels present a time offset lies in their different structure and length. For example, Ammonium and Sodium are detected much further (in terms of distance) from the melthead, when compared to dust and conductivity. This means that it will take a longer time for $[NH_4^+]$ and $[Na^+]$ to reach the detecting device and there will be a delay with respect to dust and conductivity.
Once the four records are aligned, we can remove all the artificial features that we find in the signals, as for example the high and narrow negative spikes caused by air bubbles or contamination peaks in correspondence to the top and the bottom of the core or to breaks. We also have to adjust for little portions of lost ice, which has been cut away during the cutting and cleaning stages.
Finally, the filtered and calibrated data are put on a depth scale and saved in files, with different depth resolutions (here 1 mm, 1 cm and 2 cm). Such data can be

[2] This synchronization refers to relative delays between measured components.

directly compared to the available Bern CFA data[3] and to the visual stratigraphy[4] record (VS). In figure 4.3 we show the dust records measured in CPH (blue line), Bern (red line), and the VS record of the same section of glacial ice from a depth of about 2703.5 m. An overview of all the processed data (Copenhagen CFA

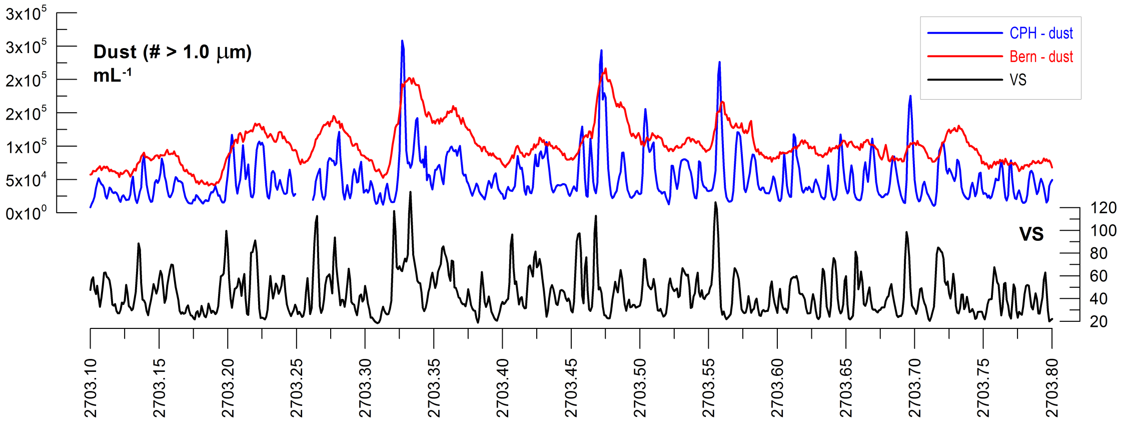

Figure 4.3: This figure shows the dust records measured in CPH (blue line), Bern (red line), and the VS record of the same section of glacial ice from a depth of about 2703.5 m. Comparing the two CFA records, we see the different resolutions provided by the CPH and the Bern systems. Nevertheless, a matching of the two records is possible and shows a good agreement between them, taking into account that the Bern curve is smoother. Moreover the CPH dust record agrees also with the VS record, whereas small shifts are sometimes visible, due to adjustments in the synchronization stage.

system, 2011), together with the VS record (black line), is given in figure 4.4. The four CFA measurements are shown along the whole depth interval analyzed in this work (2679-2730 m), with a 1-mm resolution. Dust (and the VS record) shows an evident and abrupt rise in the number of detected particles (increasing by a factor of 2-3), approximately at a depth of 2687.30 m, in correspondence to the transition from the cold GS 22 into the warmer GI 21. The opposite phenomenon seems to occur around a depth of 2718 m, entering GS 22, but more gradually than between GS 22 and GI 21, as typical for Greenland Dansgaard-Oeschger events. The same

[3] The Bern data [Ruth, 2003; Bigler, 2011] were measured using piece n. 3 of the NGRIP ice core (see fig. 4.1). Hence measurements from Bern and Copenhagen are achieved on almost identical ice samples.

[4] [Svensson et al., 2005]

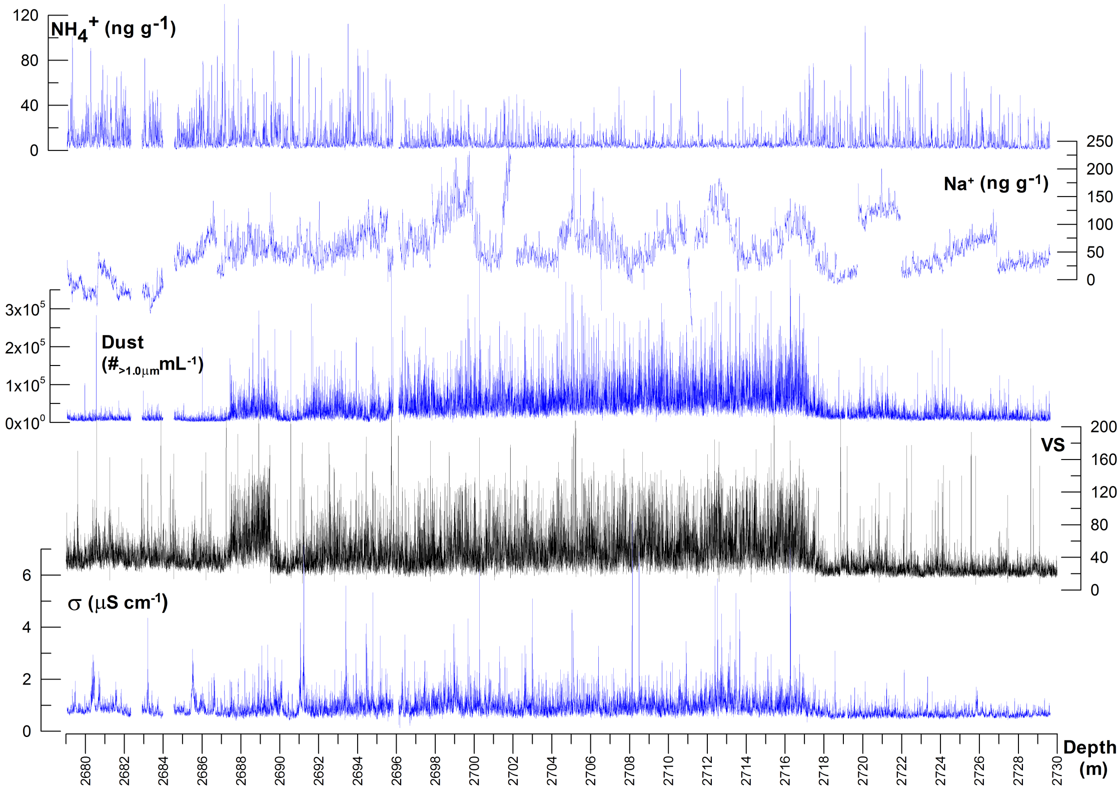

Figure 4.4: Overview of all the processed data (blue lines, Copenhagen CFA system, 2011), together with the VS record (black line, [Svensson et al., 2005]). The four CFA measurements are shown with a 1-mm resolution for the full depth interval 2679-2730 m.

characteristics, but in a less pronounced way, are seen in conductivity and, with opposite signs, in ammonium. Sodium shows evident calibration issues and a very noisy signal that makes it impossible for us to see the two transitions.

4.4 Layer counting and results

Now, as the main goal of this work, we will provide an estimation of the duration of GS 22. Layer counting is one of the most accurate techniques to date time intervals, i.e. a difference between ages, even if so far back in time (GS 22 lies between 84 kyr b2k and 88 kyr b2k, according to GICC05modelext and the NALPS record). The reason is that it does not depend on absolute dating, but only on differential counting. The layer counting technique has been presented in section

2.2, where the GICC05modelext chronology was introduced.
Our counting is mainly based on three records: the dust and the conductivity measurements achieved with the Copenhagen CFA system[5], and the visual stratigraphy record (fig. 4.5). We also used Ammonium, but mostly in the warmer periods, before and after GS 22, when it could just resolve annual layers, while during the cold period GS 22 its resolution was too low. The reason is that in cold periods accumulation is lower. Finally, the Sodium record was not used because its signal was affected by large diffusion and a high level of noise. The different resolution of dust and conductivity, compared with that of ammonium and sodium, is due to a more complex structure of the detecting lines of the latter [Bigler et al., 2011]. The counting was performed independently by three investigators (AS, PV and

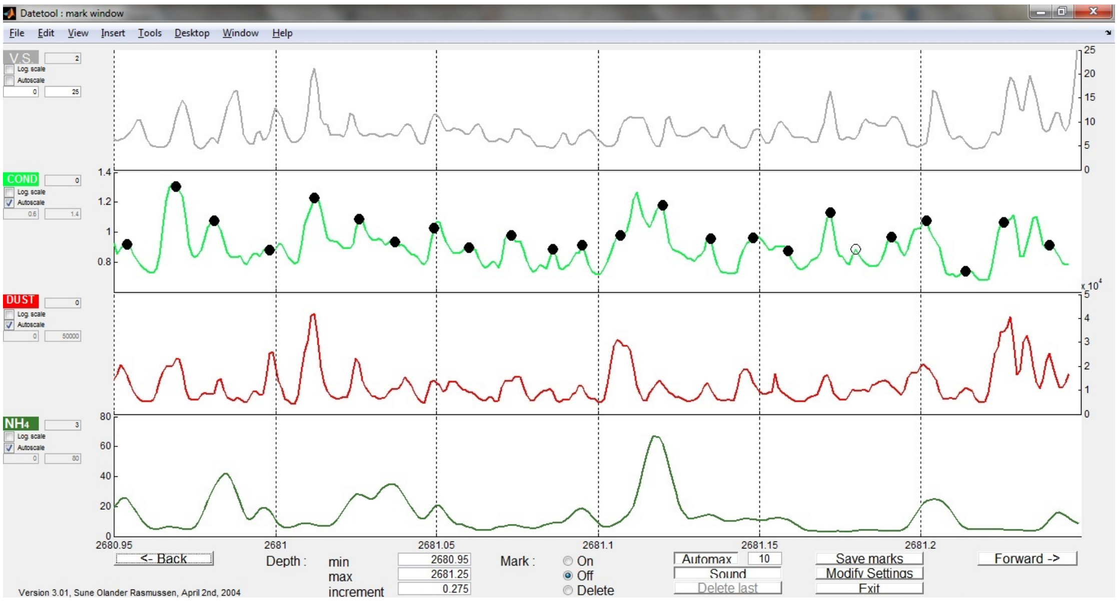

Figure 4.5: Example of a section of GI 21 (warm period following GS 22) showing, from the top to the bottom, the visual stratigraphy, the conductivity, the dust and the ammonium records used for the annual layer counting.

GB), who placed black marks (certain years, $p > 75\%$) and white marks (uncertain years, $25\% < p < 75\%$) along the whole depth interval (2679.05 - 2729.65

[5]The provided data confirmed that this CFA setup is able to detect extremely thin layers, well beneath the 10 mm threshold, providing a high resolution signal throughout the whole cold GS 22, at least in dust and conductivity.

m), using a dedicated MATLAB software (Datetool2, Version 3.01, Sune Olander Rasmussen, April 2nd, 2004). Afterwards they went through the whole counted record, discussing all the points where disagreement was found. The final counting profile results from this discussion and contains white marks (uncertain years, 0.5 $\pm$ 0.5 yr) only where no agreement could be reached. Overall, 4931.5 yr were counted, with a maximum counted error (MCE) of $\pm$ 307.5 yr.

As a next stage, we will identify the depth interval corresponding to Greenland

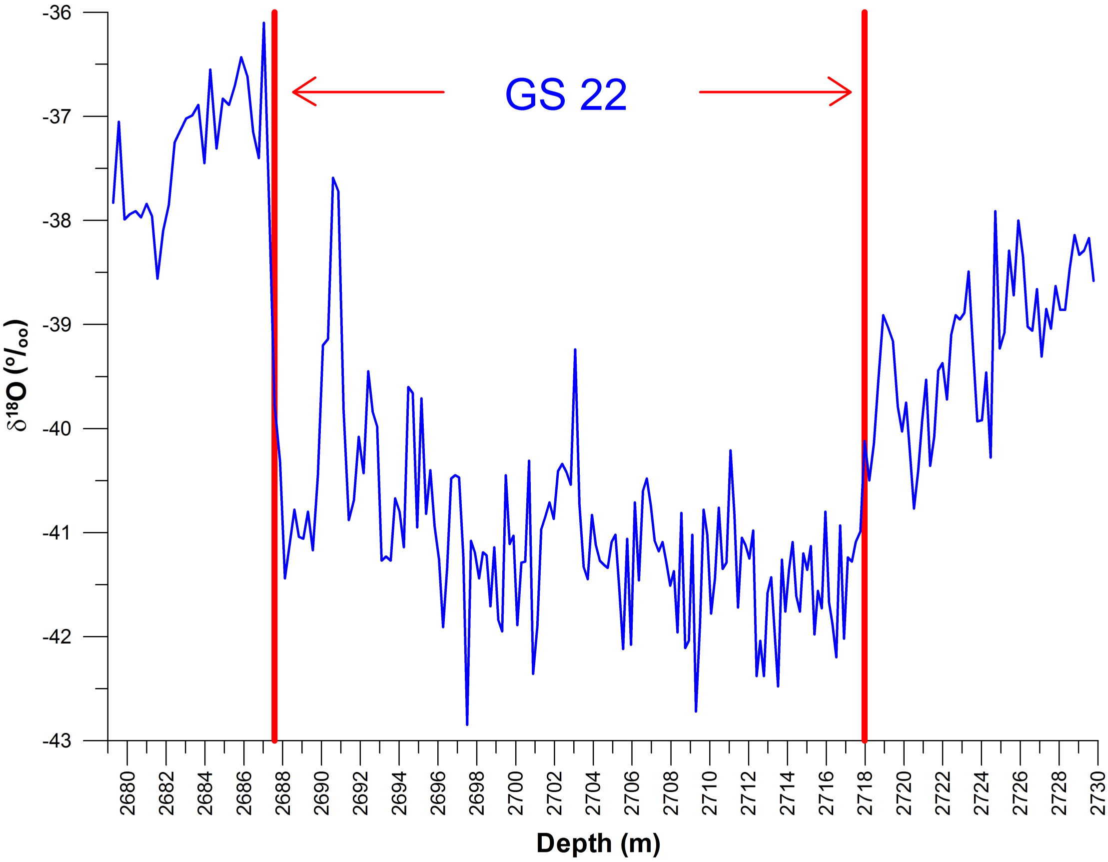

Figure 4.6: δ^{18}O profile from GICC05modelext for the depth interval 2679.05 - 2729.65 m. The red vertical bars indicate the boundaries of GS 22, i.e. the mid-points of the transitions preceding and following GS 22.

Stadial 22 in order to provide an estimation of its duration, and, later, to compare it with other independent estimations, as for example the NALPS speleothem record. Figure 4.6 shows the GICC05modelext δ^{18}O profile for the depth interval

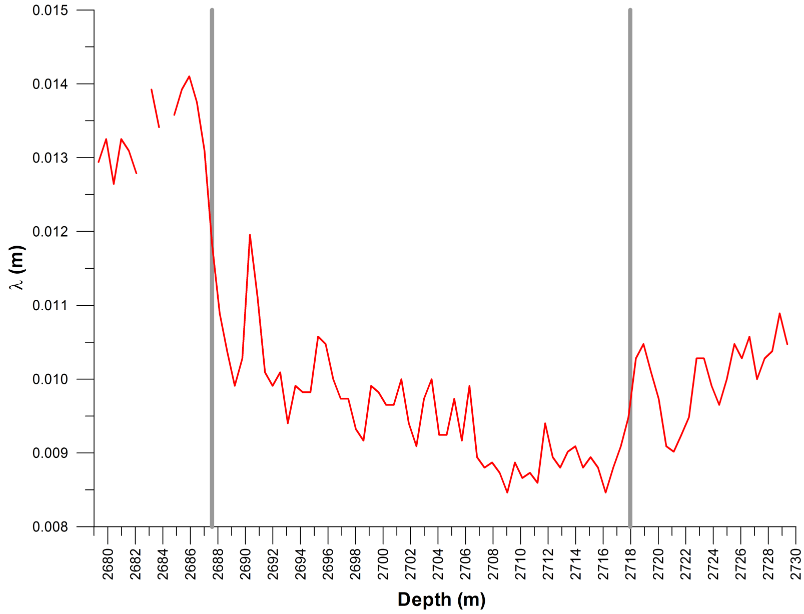

Figure 4.7: Layer thickness profile as calculated from our annual layer counting before, during and after GS 22.

investigated in this work. It also shows two red vertical bars indicating the boundaries of GS 22. We chose these boundaries by identifying the two abrupt δ^{18}O transitions preceding and following GS 22 and placing the two reference depths in the mid-points of the transitions. Such calculated depths are 2687.58 m and 2717.97 m. Finally we are able to calculate our estimate of GS 22 duration, which turns out to be 3205 yr with a MCE of ± 214 yr, equivalent to an uncertainty of 6.7%.

From our counting we can calculate a layer thickness profile, which we show in figure 4.7.

Chapter 5

Discussion and conclusions

5.1 Comparisons with GICC05modelext, NALPS, EDC and EDML (Antarctica)

In this section we will compare our CFA results about GS 22 with the timescale GICC05modelext (which, beyond 60 kyr b2k, coincides with the ss09sea model, shifted by 705 yr [Wolff et al., 2010] and with the NALPS stalagmite record [Boch et al., 2011]. We will also show a visual comparison of GS 22 and its duration with two Antarctic records, EDC3[1], and EDML[2], but a more rigorous comparison between the two hemispheres exceeds the goal of this work.

The most interesting result we can compare with other independent estimates is the duration of GS 22, which we determined to last 3205 ± 214 yr. The recently published NALPS stalagmite record [Boch et al., 2011], covering discontinuously the interval 120-60 kyr BP, originates from the Alps, where a direct comparison with Greenland in terms of oxygen isotopic composition is possible [Grafenstein et al., 1999, Spotl and Mangini, 2002]. This comparison is shown in fig. 5.1, where the GICC05modelext and the NALPS δ^{18}O profiles are plotted on their own age scales, in order to compare their shapes. We can recognize the two transitions easily and also a few smaller features which characterize GS 22, as the high peak

[1] EDC3 is the chronology for EPICA Dome C core (3rd version) [Parrenin et al., 2007].

[2] EPICA Dronning Maud Land, another drilling site in Antarctica.

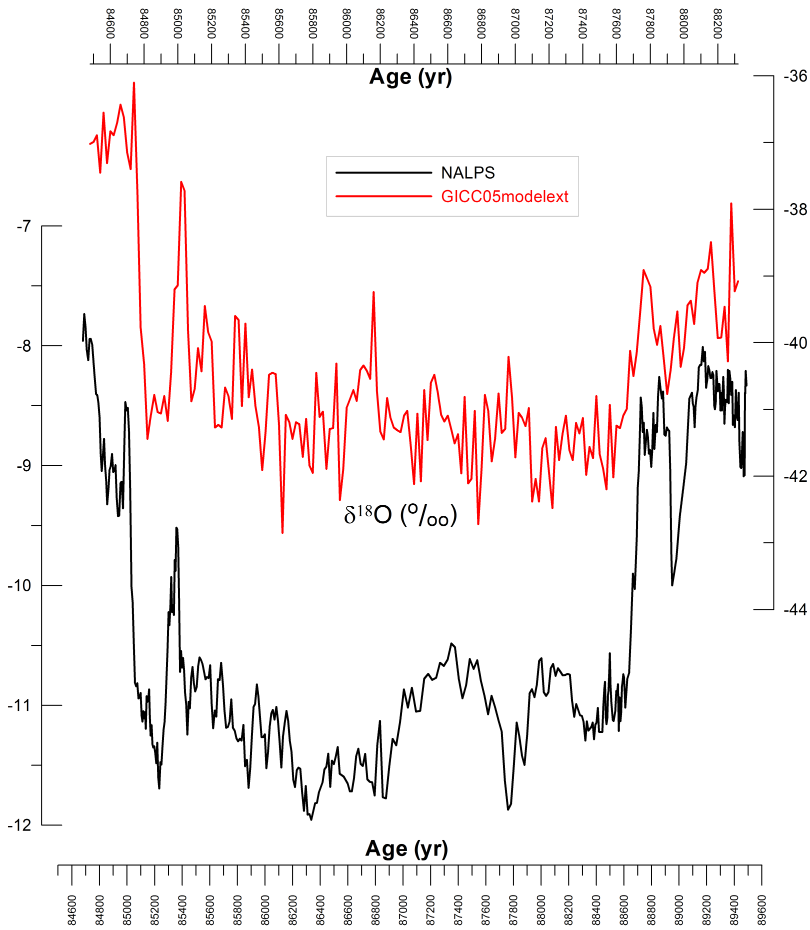

Figure 5.1: Comparison between the GICC05modelext and the NALPS δ^{18}O records (NALPS data from [Boch et al., 2011]).

preceding the cold-to-warm transition into GI 21, which is present in both records. Now we can compare the GS 22 duration estimate provided by Boch et al. [2011] with ours and with that provided by the GICC05modelext timescale. These numbers are summarized in the table of figure 5.2. The error for the NALPS estimate was calculated using uncertainty propagation. As we see, our estimation and the one provided by NALPS differ from each other by 445 years, a relevant disagreement, but they are consistent within the errors. On the other hand, the number given by GICC05modelext is not consistent with the CFA estimation.
Then we compare the layer thickness (λ) profile obtained from our CFA system with the one provided by the GICC05modelext timescale (fig. 5.3). We see that

method	t_{in}	t_{fin}	duration	error
GICC05modelext	87630	84730	2900	/
CPH-CFA	/	/	3205	214 (MCE)
NALPS	88690 ± 330	85030 ± 410	3650	526 (2σ)

Figure 5.2: Comparison between three different independent estimates for the duration of GS 22 (NALPS data from [Boch et al., 2011]) with relative errors. t_{in} stands for "initial time" (i.e. cooling transition) and t_{fin} stands for "final time" (warming transition).

the model overestimates λ throughout the whole depth interval, whereas the agreement for the main features of the profiles is good.

Now we want to show how the Antarctic equivalent of GS 22 looks like

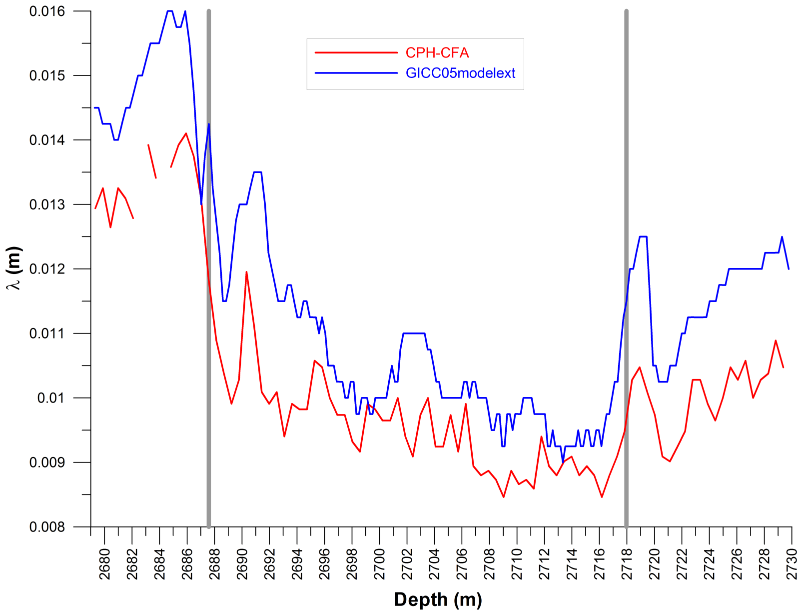

Figure 5.3: Comparison between the GICC05modelext (blue line) and the CPH-CFA (red line) layer thickness profiles. The gray vertical bars indicate the two climatic transitions.

in the Antarctic ice core records. Figure 5.4 shows how a correspondence between Dansgaard-Oeschger events in Greenland and the Antarctic Isotope Maxima (AIM) can be found, according to the thermal bipolar seesaw model [Stocker and Johnsen, 2003], which "postulates that abrupt shutdowns and initiations of the Atlantic meridional overturning circulation produce slow warmings and coolings in the Southern Ocean and Antarctic region" [Jouzel et al., 2007]. To synchronize

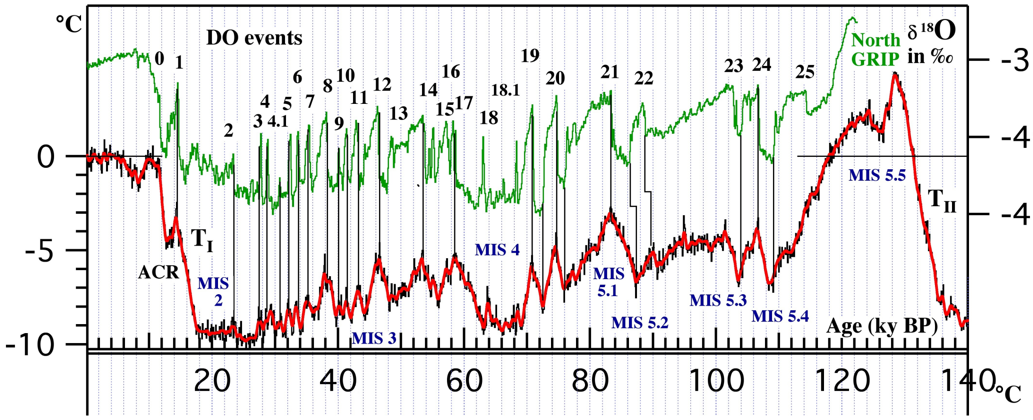

Figure 5.4: $\delta^{18}O$ profile of NorthGRIP and temperature change profile of EPICA Dome C. A correspondence between Dansgaard-Oeschger events in Greenland and the Antarctic Isotope Maxima (AIM) seems to exist, supporting the hypothesis of the thermal bipolar seesaw [Stocker and Johnsen, 2003]. Figure modified from [Jouzel et al., 2007]

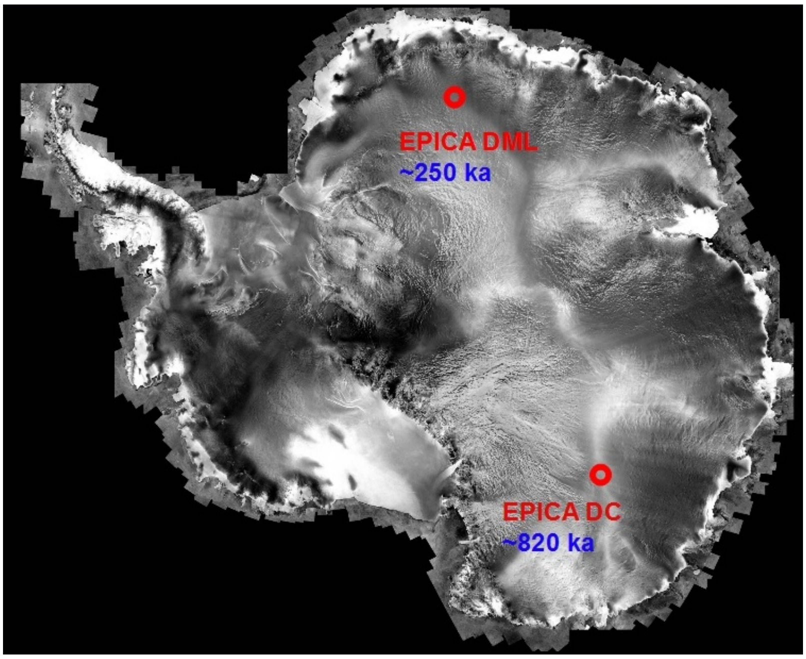

Figure 5.5: Map of Greenland showing the location of EPICA Dome C and EPICA Dronning Maud Land.

records from the two hemispheres, methane profiles are used [EPICA-members et al., 2006, Capron et al., 2010], because methane is a well-mixed gas carrying

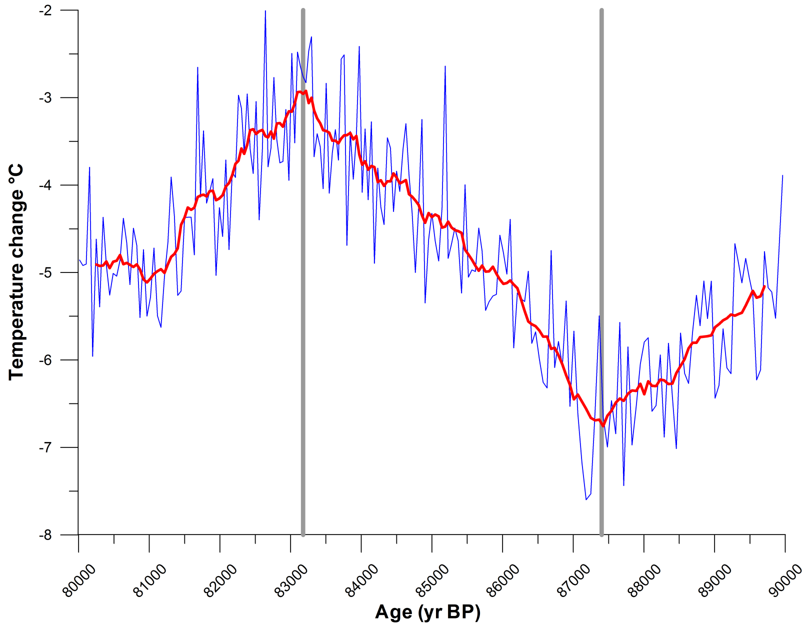

Figure 5.6: GS-22-equivalent event in Antarctica, EPICA Dome C, according to the bipolar seesaw model. Data from Jouzel et al. [2007] plotted on the EDC3 timescale [Parrenin et al., 2007]. The raw temperature change signal (blue line) was smoothed using an 11-points running average (red line).

a global signal. Hence, a comparison of the duration of GS 22 is theoretically possible, as long as we match the cooling trend with the minimum in Antarctic temperature change[3], and the warming trend with its maximum (maximum and minimum in temperature change for the EDC record are shown in figure 5.6). We plotted the Antarctic temperature change record [Jouzel et al., 2007] on the EDC3 timescale [Parrenin et al., 2007] and then identified the maximum and the minimum values around the supposed GS-22-equivalent Antarctic event. This is shown as a smoothed curve (red line, 11-points running average), because the raw temperature data were too noisy. This preliminary visual estimation gives about 4224 yr, thus suggesting a much longer duration for the Antarctic counterpart of GS 22 at EPICA Dome C.
An analogous comparison can be made with EDML, a drilling site (figure 5.5) characterized by larger accumulation rates than EPICA Dome C (EDC) and, thus,

[3] Temperatures as reconstructed from the stable isotopes records.

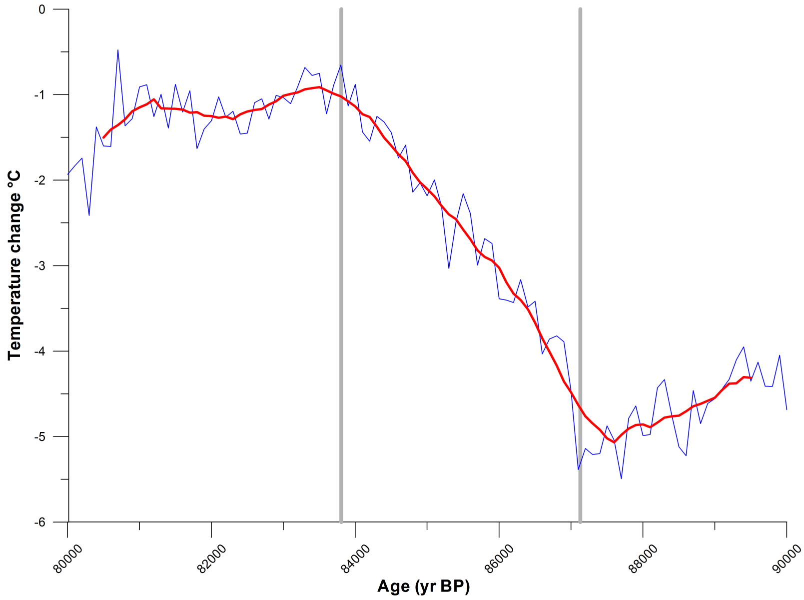

Figure 5.7: GS-22-equivalent event in Antarctica, EPICA Dronning Maud Land, according to the bipolar seesaw model. Data from EPICA-members et al. [2006] plotted on the EDML1 timescale [Ruth et al., 2007]. The raw temperature change signal (blue line) was smoothed using an 11-points running average (red line).

more suitable for a comparison with NGRIP in a deep section as is GS 22. Figure 5.7 shows the EDML temperature change record corresponding to AIM 21 (Antarctic Isotope Maximum 21, corresponding to Greenland Stadial GS 22). The grey vertical bars indicate the boundaries of AIM 21 (identified by the minimum and the maximum in temperature change) and were used to estimate its duration, resulting in 3324 yr. (consistent with our counting within the uncertainty).
Finally, the linear dependence of the AIMs temperature amplitude and the duration of the corresponding Stadial of the northern hemisphere, showed by EPICA-members et al. [2006] for MIS 3[4] and based on the thermal bipolar seesaw model, was tested for GS 22/AIM 21, belonging to MIS 5. Using 3205 yr for the GS 22 duration and 4.7 °C as a difference in temperature change leading to AIM 21, we obtain the point labeled with "21" in figure 5.8. Hence, this result supports the thermal bipolar seesaw model.

[4]Marine Isotope Stage 3, derived from planktonik foraminifera

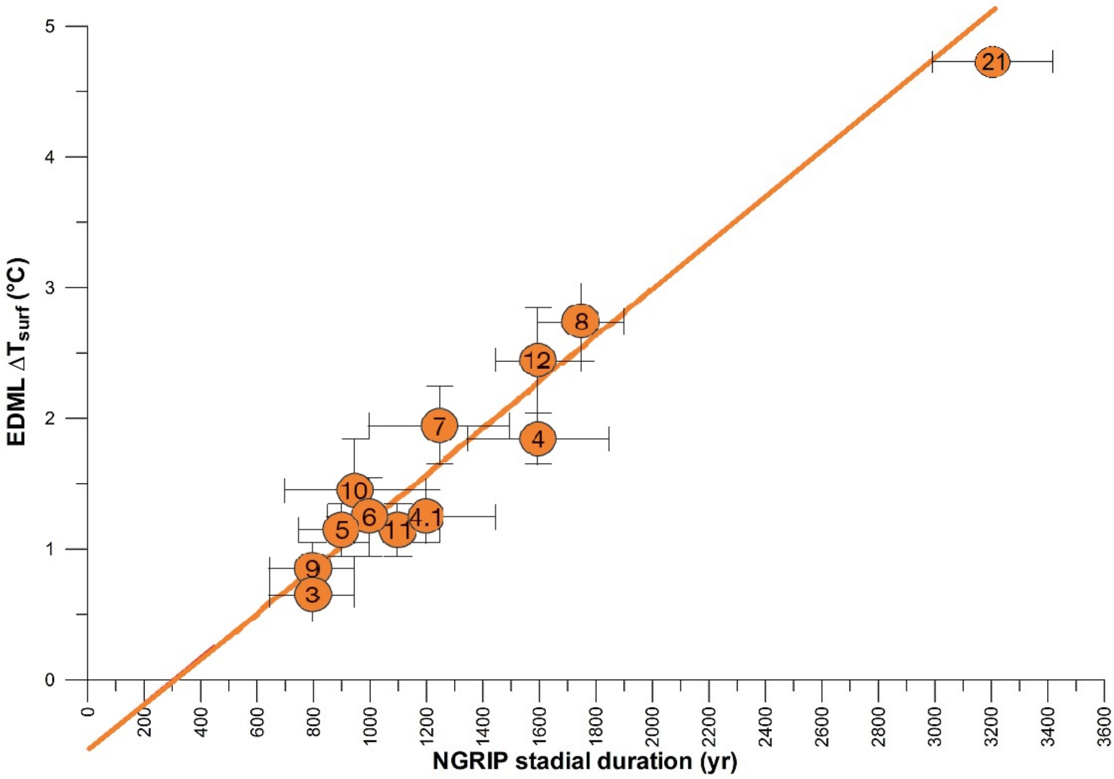

Figure 5.8: The linear dependence of the AIMs temperature amplitude and the duration of the corresponding Stadial of the northern hemisphere, showed by EPICA-members et al. [2006] for MIS 3, was tested for GS 22/AIM 21 (MIS 5). Figure modified from EPICA-members et al. [2006].

5.2 Conclusions

The main aim of this work is to provide an independent, layer-counted estimation of the duration of Greenland Stadial 22, in order to shed light on the discrepancies observed between the model-based chronology ss09sea (and consequently GICC05modelext), the recently published stalagmite record NALPS and, also, the Antarctic records of EDC and EDML, in correspondence to this cold period of the last glacial era. With this intent, we conducted Continuous Flow Analysis measurements of insoluble dust particles, electrical conductivity, ammonium concentration and sodium concentration of meltwater from the corresponding North

Greenland Ice Core Project (NGRIP) ice section. With the CFA system of the Centre for Ice and Climate, Copenhagen, we were able to resolve extremely thin layers, down to a thickness of 5-10 mm. This improved high resolution setup enabled us to perform an almost complete layer counting throughout the investigated depth interval (NGRIP, 2679-2730m), based on seasonal signals of the above mentioned species. This has not been done before with ice older than 80 kyr and represents a clear step forward in high resolution impurities analysis. This newly layer-counted cold period represents a further contribution to the existing GICC05 (entirely layer-counted) chronology for the NGRIP ice core, which, at present, covers the last 60 kyr. This work shows that it is possible to resolve annual layers even in glacial cold ice, back to 84-88 ky b2k, and, potentially, back to the Eemian (last interglacial). The comparison between the layer-counted duration of GS 22 and that calculated by the ss09sea model suggests that the latter is overestimating annual layer thicknesses throughout the investigated depth-time interval. This view is further supported by the NALPS record, which provides an even longer duration estimate for GS 22.

The possibility of matching and synchronizing more independently measured signals and chronologies is one of the major aims of climate studies. Comparison of this CFA data set with the NALPS speleothem record shows that climate proxies such as δ^{18}O are recoverable, with very similar profiles, in records originating from completely different dynamics, environments and regions of the northern hemisphere. Furthermore, works like this can improve our knowledge about the onset of the abrupt climatic transitions called Dansgaard-Oeschger events, occurring along the whole last glacial, and can help us finding the Antarctic counterpart of them and the connections between northern and southern hemispheres. Our comparison of the GS 22 duration with the EDML record seems to support the thermal bipolar seesaw model, confirming, for GS 22, the linear dependence between the AIMs temperature amplitude and the duration of the corresponding Stadial of the northern hemisphere. Furthermore, an approximated estimation of the duration of AIM 21 (corresponding to GS 22) in the Antarctic record of EDML shows a good agreement with our estimation for the GS 22 duration, whereas an analogous comparison with an estimation based on EDC shows a difference of about 1000 yr. The two Antarctic ice cores present different characteristics, such as the accumulation rate which in EDML is more than twice that of EDC, leading the former core to be a more suitable candidate for the comparison with NGRIP.

This results indicate one possible way to follow to improve our knowledge about the climate of last glacial in Greenland and to investigate the connection between the climate dynamics of the two hemispheres. The former aim can be achieved by completing the existing layer-counted chronology GICC05 for Greenland back to the Eemian, using high-resolution impurities analysis as that presented in this work, and matching different records by identifying new volcanic horizons and other recognizable global events.

Bibliography

K.K. Andersen, A. Svensson, S.J. Johnsen, S.O. Rasmussen, M. Bigler, R. Röthlisberger, U. Ruth, M.L. Siggaard-Andersen, J. Peder Steffensen, D. Dahl-Jensen, et al. The greenland ice core chronology 2005, 15-42 ka. part 1: constructing the time scale. *Quaternary Science Reviews*, 25(23-24):3246–3257, 2006.

M. Bigler, A. Svensson, J.P. Steffensen, and P. Kaufmann. A new continuous high-resolution detection system for sulphate in ice cores. *Annals of Glaciology*, 45(1):178–182, 2007.

M. Bigler, A. Svensson, E. Kettner, P. Vallelonga, M.E. Nielsen, and J.P. Steffensen. Optimization of high-resolution continuous flow analysis for transient climate signals in ice cores. *Environmental science & technology*, 2011.

P.E. Biscaye, F.E. Grousset, M. Revel, S. Van der Gaast, G.A. Zielinski, A. Vaars, and G. Kukla. Asian provenance of glacial dust (stage 2) in the greenland ice sheet project 2 ice core, summit, greenland. *Journal of Geophysical Research*, 102(C12):26765–26, 1997.

R. Boch, H. Cheng, C. Spötl, R. L. Edwards, X. Wang, and Ph. Häuselmann. Nalps: a precisely dated european climate record 120–60 ka. *Climate of the Past*, 7(4):1247–1259, 2011. doi: 10.5194/cp-7-1247-2011. URL `http://www.clim-past.net/7/1247/2011/`.

E. Capron, A. Landais, B. Lemieux-Dudon, A. Schilt, V. Masson-Delmotte, D. Buiron, J. Chappellaz, D. Dahl-Jensen, S. Johnsen, M. Leuenberger, et al. Synchronising edml and northgrip ice cores using [delta] 18o of atmospheric oxygen ([delta] 18oatm) and ch4 measurements over mis5 (80-123 kyr). *Quaternary Science Reviews*, 29(1-2):222–234, 2010.

C.D. Charles, D. Rind, J. Jouzel, R.D. Koster, and R.G. Fairbanks. Glacial-interglacial changes in moisture sources for greenland: Influences on the ice core record of climate. *Science*, 263(5146):508, 1994.

D. Dahl-Jensen, N. Gundestrup, S.P. Gogineni, and H. Miller. Basal melt at northgrip modeled from borehole, ice-core and radio-echo sounder observations. *Annals of Glaciology*, 37(1):207–212, 2003.

W. Dansgaard. The abundance of o18 in atmospheric water and water vapour. *Tellus*, 5(4):461–469, 1953.

W. Dansgaard. The isotopic composition of natural waters with special reference to the greenland ice cap. Technical report, Oersted Inst., Copenhagen, 1961.

W. Dansgaard. Stable isotopes in precipitation. *Tellus*, 16(4):436–468, 1964.

J.E. Dibb and J.L. Jaffrezo. Air-snow exchange investigations at summit, greenland: An overview. *JOURNAL OF GEOPHYSICAL RESEARCH-ALL SERIES-*, 102:26–26, 1997.

EPICA-members, C. Barbante, J.M. Barnola, S. Becagli, J. Beer, M. Bigler, C. Boutron, T. Blunier, E. Castellano, O. Cattani, J. Chappellaz, et al. One-to-one coupling of glacial climate variability in greenland and antarctica. *Nature*, 444(7116):195–198, 2006.

H. Fischer, M.L. Siggaard-Andersen, U. Ruth, R. Rothlisberger, and E. 4. Glacial/interglacial changes in mineral dust and sea-salt records in polar ice cores: Sources, transport, and deposition. *Reviews of geophysics*, 45(1), 2007.

A. Fuchs and M.C. Leuenberger. δ18o of atmospheric oxygen measured on the grip ice core document stratigraphic disturbances in the lowest 10% of the core. *Geophysical Research Letters*, 23(9):1049–1052, 1996.

K. Fuhrer, A. Neftel, M. Anklin, T. Staffelbach, and M. Legrand. High-resolution ammonium ice core record covering a complete glacial-interglacial cycle. *Journal of Geophysical Research*, 101(D2):4147–4164, 1996.

U. Grafenstein, H. Erlenkeuser, A. Brauer, J. Jouzel, and S.J. Johnsen. A mid-european decadal isotope-climate record from 15,500 to 5000 years bp. *Science*, 284(5420):1654, 1999.

A. Grinsted and D. Dahl-Jensen. A monte carlo-tuned model of the flow in the northgrip area. *Annals of Glaciology*, 35(1):527–530, 2002.

P.M. Grootes, M. Stuiver, J.W.C. White, S. Johnsen, and J. Jouzel. Comparison of oxygen isotope records from the gisp2 and grip greenland ice cores. 1993.

C.U. Hammer. Acidity of polar ice cores in relation to absolute dating, past volcanism, and radio-echoes. *Journal of Glaciology*, 25:359–372, 1980.

C.U. Hammer. Dating by physical and chemical seasonal variations and reference horizons. *The Environmental Record in Glaciers and Ice Sheets, Ed. by Oeschger H and Langway CCJr, John Wiley&Sons Limited*, pages 99–121, 1989.

C.U. Hammer, K.K. Andersen, H.B. Clausen, D. Dahl-Jensen, C.S. Hvidberg, and P. Iversen. The stratigraphic dating of the grip ice core. *Special Report of the Geophysical Department, Niels Bohr Institute for Astronomy, Physics and Geophysics, University of Copenhagen, GRIP-GISP CD-ROM (" le gripstrt)*, 1997.

S.J. Johnsen, H.B. Clausen, W. Dansgaard, K. Fuhrer, N. Gundestrup, C.U. Hammer, P. Iversen, J. Jouzel, B. Stauffer, and J.P. Steffensen. Irregular glacial interstadials recorded in a new greenland ice core. *Nature*, 359(6393):311–313, 1992.

S.J. Johnsen, D. DAHL-JENSEN, W. Dansgaard, and N. Gundestrup. Greenland palaeotemperatures derived from grip bore hole temperature and ice core isotope profiles. *Tellus B*, 47(5):624–629, 1995.

S.J. Johnsen, D. Dahl-Jensen, N. Gundestrup, J.P. Steffensen, H.B. Clausen, H. Miller, V. Masson-Delmotte, A.E. Sveinbjörnsdottir, and J. White. Oxygen isotope and palaeotemperature records from six greenland ice-core stations: Camp century, dye-3, grip, gisp2, renland and northgrip. *Journal of Quaternary Science*, 16(4):299–307, 2001.

J. Jouzel, V. Masson-Delmotte, O. Cattani, G. Dreyfus, S. Falourd, G. Hoffmann, B. Minster, J. Nouet, J.M. Barnola, J. Chappellaz, et al. Orbital and millennial antarctic climate variability over the past 800,000 years. *science*, 317(5839):793, 2007.

P.R. Kaufmann, U. Federer, M.A. Hutterli, M. Bigler, S. Schüpbach, U. Ruth, J. Schmitt, and T.F. Stocker. An improved continuous flow analysis system for high-resolution field measurements on ice cores. *Environmental science & technology*, 42(21):8044–8050, 2008.

C.C. Langway. Stratigraphic analysis of a deep ice core from greenland. *1967*, 1967.

D.G. Martinson, N.G. Pisias, J.D. Hays, J. Imbrie, T.C. Moore, N.J. Shackleton, et al. Age dating and the orbital theory of the ice ages: development of a high-resolution 0 to 300,000-year chronostratigraphy. *Quaternary research*, 27 (1):1–29, 1987.

V. Masson-Delmotte, J. Jouzel, A. Landais, M. Stievenard, S.J. Johnsen, JWC White, M. Werner, A. Sveinbjornsdottir, and K. Fuhrer. Grip deuterium excess reveals rapid and orbital-scale changes in greenland moisture origin. *Science*, 309(5731):118, 2005.

NGRIP-members, K.K. Andersen, N. Azuma, J.M. Barnola, M. Bigler, P. Biscaye, N. Caillon, J. Chappellaz, HB Clausen, D. Dahl-Jensen, H. Fischer, et al. High-resolution record of northern hemisphere climate extending into the last interglacial period. *Nature*, 431(7005):147–151, 2004.

M.E. Nielsen. Early holocene and eemian impurity profiles from the ngrip ice core. *Master Project*, 2009.

F. Parrenin, J.M. Barnola, J. Beer, T. Blunier, E. Castellano, J. Chappellaz, G. Dreyfus, H. Fischer, S. Fujita, J. Jouzel, et al. The edc3 chronology for the epica dome c ice core. *Climate of the Past*, 3:485–497, 2007.

S.O. Rasmussen, K.K. Andersen, A.M. Svensson, J.P. Steffensen, B.M. Vinther, H.B. Clausen, M.L. Siggaard-Andersen, S.J. Johnsen, L.B. Larsen, D. Dahl-Jensen, et al. A new greenland ice core chronology for the last glacial termination. *Journal of geophysical research*, 111(D6):D06102, 2006.

R. Röthlisberger, M. Bigler, M. Hutterli, S. Sommer, B. Stauffer, H.G. Junghans, and D. Wagenbach. Technique for continuous high-resolution analysis of trace substances in firn and ice cores. *Environmental science & technology*, 34(2): 338–342, 2000.

U. Ruth, D. Wagenbach, J.P. Steffensen, and M. Bigler. Continuous record of microparticle concentration and size distribution in the central greenland ngrip ice core during the last glacial period. *J. Geophys. Res*, 108(10.1029), 2003.

U. Ruth, J.M. Barnola, J. Beer, M. Bigler, T. Blunier, E. Castellano, H. Fischer, F. Fundel, P. Huybrechts, P. Kaufmann, et al. 'edml1': a chronology for the epica deep ice core from dronning maud land, antarctica, over the last 150 000 years. *Climate of the Past Discussions*, 3(2):549–574, 2007.

U. Ruth, C. Barbante, M. Bigler, B. Delmonte, H. Fischer, P. Gabrielli, V. Gaspari, P. Kaufmann, F. Lambert, V. Maggi, et al. Proxies and measurement techniques for mineral dust in antarctic ice cores. *Environmental science & technology*, 42 (15):5675–5681, 2008.

J. Schwander, J. Jouzel, C.U. Hammer, J.R. Petit, R. Udisti, and E. Wolff. A tentative chronology for the epica dome concordia ice core. *Geophysical research letters*, 28(22):4243–4246, 2001.

J. Southon. A radiocarbon perspective on greenland ice-core chronologies: can we use ice cores for 14c calibration. *Radiocarbon*, 46(3):1239–1260, 2004.

C. Spotl and A. Mangini. Stalagmite from the austrian alps reveals dansgaard-oeschger events during isotope stage 3::: Implications for the absolute chronology of greenland ice cores. *Earth and Planetary Science Letters*, 203(1):507–518, 2002.

B. Stauffer, G. Fischer, A. Neftel, and H. Oeschger. Increase of atmospheric methane recorded in antarctic ice core. *Science*, 229(4720):1386, 1985.

T.F. Stocker and S.J. Johnsen. A minimum thermodynamic model for the bipolar seesaw. *Paleoceanography*, 18(4):1087, 2003.

A. Svensson, S.W. Nielsen, S. Kipfstuhl, S.J. Johnsen, J.P. Steffensen, M. Bigler, U. Ruth, and R. Röthlisberger. Visual stratigraphy of the north greenland ice core project (northgrip) ice core during the last glacial period. *Journal of Geophysical Research*, 110(D2):D02108, 2005.

A. Svensson, K.K. Andersen, M. Bigler, H.B. Clausen, D. Dahl-Jensen, S.M. Davies, S.J. Johnsen, R. Muscheler, S.O. Rasmussen, R. Röthlisberger, et al. The greenland ice core chronology 2005, 15-42 ka. part 2: Comparison to other records. *Quaternary Science Reviews*, 25(23-24):3258–3267, 2006.

A. Svensson, K.K. Andersen, M. Bigler, H.B. Clausen, D. Dahl-Jensen, SM Davies, S.J. Johnsen, R. Muscheler, F. Parrenin, S.O. Rasmussen, et al. A 60 000 year greenland stratigraphic ice core chronology. *Climate of the Past*, 4(1):47–57, 2008.

B.M. Vinther, H.B. Clausen, S.J. Johnsen, S.O. Rasmussen, K.K. Andersen, S.L. Buchardt, D. Dahl-Jensen, I.K. Seierstad, ML Siggaard-Andersen, J.P. Steffensen, et al. A synchronized dating of three greenland ice cores throughout the holocene. *Journal of Geophysical Research*, 111(D13):1–11, 2006.

E.W. Wolff, J. Chappellaz, T. Blunier, S.O. Rasmussen, and A. Svensson. Millennial-scale variability during the last glacial: The ice core record. *Quaternary Science Reviews*, 29(21-22):2828–2838, 2010.

List of Figures

1.1 The schematic structure of the Greenland ice sheet showing the flow of ice from the top toward the bottom and the lateral margins, where it is released through ablation (melting and icebergs calving). 14

1.2 δ^{18}O profile of Greenland NGRIP ice [A. Svensson, pers. comm.]. . 16

1.3 Scheme of the densification process that transforms snow into ice, first passing through an intermediate stage called firn. 17

1.4 ECM (Electrical Conductivity Measurement) is measured by putting a pair of anode and cathode on the flat surface of ice and moving them slowly along the core, thus, providing a continuous ECM record [Hammer, 1980]. 20

1.5 Map of Greenland, showing the locations of the deep ice core drilling sites (NGRIP-members et al. [2004] modified). 21

1.6 Comparison between two configurations: with and without basal melting. 22

1.7 The δ^{18}O profile of NorthGRIP and the temperature change profile of EPICA Dome C (an ice core from Antarctica) are shown here. A correspondence between Dansgaard-Oeschger events in Greenland and the Antarctic Isotope Maxima (AIM) seems to exist, supporting the hypothesis of the thermal bipolar seesaw [Stocker and Johnsen, 2003]. Figure modified from [Jouzel et al., 2007] 23

1.8 Greenland Stadial 22 as recorded by the NALPS stalagmites BA1 and BA2, modified from [Boch et al., 2011]. The horizontal error bars on the bottom represent the uncertainties related to the U-Th dating method. The yellow areas highlight sub-Dansgaard-Oeschger warming and cooling events. 24

1.9 NEEM-NGRIP depth-depth matchpoint correlation over the early part of last glacial [S. Rasmussen, pers. comm.]. 24

1.10 Map of the Alps showing the locations of the cave sites investigated by Boch et al. [2011]. Because of its exposure to a strong Atlantic influence, this region is suitable for a comparison with Greenland climate. 25

1.11 Comparison between the NALPS record and NGRIP (GICC05modelext timescale). The former consists of seven different stalagmites, plotted with different colors, and covers the time interval 60-120 kyr BP. The horizontal error bars on the bottom represent the uncertainties related to the U-Th dating method,while the yellow areas highlight sub-Dansgaard-Oeschger warming and cooling events. 26

2.1 Map of Greenland, showing the locations of the deep ice core drilling sites [NGRIP-members et al., 2004]. 28

2.2 Horizontal and vertical velocity profiles, $v_x(y)$ and $v_y(y)$, as assumed in the Kink Model for the ice flow used to construct the timescale ss09sea [Centre for Ice and Climate]. H is the ice thickness, y_0 the kink depth and A_H the annual accumulation. 29

2.3 These theree different ice sections from NGRIP (modified from [Svensson et al., 2005]) show very thin but regular annual layers (left), microfolding (center) and hardly distinguishable layers (right). 32

2.4 The GICC05 chronology is built with the contributions of three different ice cores - DYE-3, GRIP and NGRIP - and their multi-parameter records. All the available records are used, and here time intervals are shown, where different records overlap or are matched using ECM reference horizons, thus ensuring consistency between them [Centre for Ice and Climate]. The chronology has then been extended from present time back to 60 kyr b2k. 33

2.5 Example of layer counting performed on an early Holocene section of NGRIP (upper nine records) and GRIP (lower five records) ice. The gray vertical bars show the annual layers, that here are marked at summer peaks [Rasmussen et al., 2006]. 35

2.6 Example of annual layer counting during a Stadial. Certain/uncertain years are indicated by gray/dashed vertical bars. Here visual stratigraphy and ECM have the best resolution [Svensson et al., 2008]. . . 37

2.7 NGRIP δ^{18}O and annual layer thickness profiles according to GICC05 [Svensson et al., 2008]. 39

2.8 Distribution of annual layer thicknesses ($\lambda_{corr.}$ is the strain corrected thickness) for Stadials (red), Interstadials (yellow) and for the cold GS 2 period [Andersen et al., 2006]. 39

2.9 Comparison between the GICC05 time scale and other independently dated records. The differences between GICC05 and the other timescales are plotted in different colors, while the gray shaded area represents the GICC05 MCE, i.e. the counting uncertainty [Svensson et al., 2008]. 40

3.1 The CFA-setup at the Centre for Ice and Climate, Copenhagen. . . 42

3.2 Here we see a small section of NGRIP ice from a depth of about 2691.5 m, during the cold period called GS 22. The meltwater conductivity is shown, using the red line to represent the Bern-CFA data [Ruth et al., 2003, Bigler et al., 2011], and the blue one for our measurements, achieved with the CFA-setup in Copenhagen. The difference in resolution is easily recognizable since the Bern signal is much smoother than ours. 43

3.3 Schematic of the CFA-setup 44

3.4 The melthead with its 2-mm-high ridge dividing the melt surface into two distinct areas [Bigler et al., 2011]. 45

3.5 The debubbler. 45

3.6 The flow cell where sodium is detected (from [Nielsen, 2009]). . . . 47

4.1 Each piece of the ice core section is used for a different goal: 1) physical properties of the ice; 2) gas; 3) CFA; 4) stable isotopes and 5) on this piece electrical conductivity is measured, and then a piece identical to number 3 is obtaind, which we used for our measurements. A part of the rest of piece 5 goes to the NGRIP Archive [Centre for Ice and Climate]. 50

4.2 This figure is an example of sodium and ammonium calibration. We can see two peaks for the ammonium standards and three for sodium. 51

4.3 This figure shows the dust records measured in CPH (blue line), Bern (red line), and the VS record of the same section of glacial ice from a depth of about 2703.5 m. Comparing the two CFA records, we see the different resolutions provided by the CPH and the Bern systems. Nevertheless, a matching of the two records is possible and shows a good agreement between them, taking into account that the Bern curve is smoother. Moreover the CPH dust record agrees also with the VS record, whereas small shifts are sometimes visible, due to adjustments in the synchronization stage. 53

4.4 Overview of all the processed data (blue lines, Copenhagen CFA system, 2011), together with the VS record (black line, [Svensson et al., 2005]). The four CFA measurements are shown with a 1-mm resolution for the full depth interval 2679-2730 m. 54

4.5 Example of a section of GI 21 (warm period following GS 22) showing, from the top to the bottom, the visual stratigraphy, the conductivity, the dust and the ammonium records used for the annual layer counting. 55

4.6 δ^{18}O profile from GICC05modelext for the depth interval 2679.05 - 2729.65 m. The red vertical bars indicate the boundaries of GS 22, i.e. the mid-points of the transitions preceding and following GS 22. 56

4.7 Layer thickness profile as calculated from our annual layer counting before, during and after GS 22. 57

5.1 Comparison between the GICC05modelext and the NALPS δ^{18}O records (NALPS data from [Boch et al., 2011]). 60

5.2 Comparison between three different independent estimates for the duration of GS 22 (NALPS data from [Boch et al., 2011]) with relative errors. t_{in} stands for "initial time" (i.e. cooling transition) and t_{fin} stands for "final time" (warming transition). 61

5.3 Comparison between the GICC05modelext (blue line) and the CPH-CFA (red line) layer thickness profiles. The gray vertical bars indicate the two climatic transitions. 61

5.4 δ^{18}O profile of NorthGRIP and temperature change profile of EPICA Dome C. A correspondence between Dansgaard-Oeschger events in Greenland and the Antarctic Isotope Maxima (AIM) seems to exist, supporting the hypothesis of the thermal bipolar seesaw [Stocker and Johnsen, 2003]. Figure modified from [Jouzel et al., 2007] . . . 62

5.5 Map of Greenland showing the location of EPICA Dome C and EPICA Dronning Maud Land. 62

5.6 GS-22-equivalent event in Antarctica, EPICA Dome C, according to the bipolar seesaw model. Data from Jouzel et al. [2007] plotted on the EDC3 timescale [Parrenin et al., 2007]. The raw temperature change signal (blue line) was smoothed using an 11-points running average (red line). 63

5.7 GS-22-equivalent event in Antarctica, EPICA Dronning Maud Land, according to the bipolar seesaw model. Data from EPICA-members et al. [2006] plotted on the EDML1 timescale [Ruth et al., 2007]. The raw temperature change signal (blue line) was smoothed using an 11-points running average (red line). 64

5.8 The linear dependence of the AIMs temperature amplitude and the duration of the corresponding Stadial of the northern hemisphere, showed by EPICA-members et al. [2006] for MIS 3, was tested for GS 22/AIM 21 (MIS 5). Figure modified from EPICA-members et al. [2006]. 65